Interval Forecasting of Cryptocurrency Returns using Quantile Regression Forests: An Application to the Solana Ecosystem

Interval Forecasting of Cryptocurrency Returns using Quantile Regression Forests: An Application to the Solana Ecosystem

James Lewis

Table of contents

1 Abstract

Interval Forecasting of Cryptocurrency Returns using Quantile Regression Forests: An Application to the Solana Ecosystem

Abstract. (200–300 words placeholder) Problem, data (12-h bars; 72-h target), models (QRF, LQR, LGBM), rolling CV (120/24/6), metrics (pinball, coverage, width), key results + trading relevance.

2 Introduction

2.1 The Economic Challenge of Forecasting in Emerging Ecosystems

Extreme volatility and non-normal return distributions are defining characteristics of cryptocurrency markets, rendering traditional point forecasts insufficient for robust risk management (Gkillas and Katsiampa, 2018). This challenge is particularly acute for mid-capitalisation tokens within emerging ecosystems like Solana. Unlike large-cap assets, these tokens are subject to rapid narrative shifts and idiosyncratic on-chain dynamics; yet unlike micro-caps, they are liquid enough to attract significant capital. For participants in this space, standard risk models often fail during periods of high network activity or ecosystem-wide events, creating a clear demand for forecasting tools that can dynamically price tail risk.

This dissertation argues that the primary objective must shift from point prediction to **interval forecasting**. By generating calibrated prediction intervals through conditional quantiles, we can capture the asymmetry and tail risk inherent in these volatile assets. A well-calibrated lower quantile serves as a dynamic, forward-looking analogue to Value-at-Risk (VaR) (Engle and Manganelli, 2004), while the upper quantile informs on potential upside, providing a comprehensive basis for sophisticated risk management and tactical decision-making.

2.2 A Principled Approach: Quantile Regression

To construct reliable prediction intervals, we adopt the framework of **quantile regression** (Koenker and Bassett, 1978), evaluated with the pinball loss—a strictly proper score for quantiles. We use it throughout for model training and comparison, and provide the formal definition in the **Methodology** and Appendix 2.

This allows models to be evaluated on two critical properties: **calibration** (does an 80% interval contain the outcome 80% of the time?) and **sharpness** (are the intervals as narrow as possible while maintaining calibration?) (Gneiting and Raftery, 2007). These properties are paramount in crypto markets, where accurately quantifying both risk and opportunity is the basis of effective strategy.

2.3 The State of the Art and the Research Gap

The literature on cryptocurrency forecasting has largely bifurcated. One branch applies econometric models like GARCH, which excel at modelling volatility but are constrained by parametric assumptions (Bollerslev, 1986). The other employs machine learning, but predominantly for point forecasting of price or direction (Mcnally, Roche and Caton, 2018). While some studies have applied quantile regression to major crypto-assets (Catania and Sandholdt, 2019), they have typically relied on simpler linear models or have not fully leveraged the rich feature set available from on-chain data. Furthermore, the critical step of post-hoc calibration to ensure nominal coverage guarantees, especially for non-parametric methods, is often overlooked.

In doing so, the study prioritises distributional accuracy over point prediction, applies a non-parametric approach to a mid-cap Solana universe, and integrates market microstructure and on-chain features—choices that, as later results show, yield sharper, better-calibrated intervals than linear and boosted baselines after post-hoc calibration.

2.4 Problem Formulation: The Solana Ecosystem

This study focuses on forecasting **72-hour log-returns** for a universe of mid-cap tokens within the Solana ecosystem, using data aggregated in 12-hour intervals. The asset universe comprises tokens with a market capitalisation exceeding greater than $30 million and listing age greater than 6 months, ensuring a focus on liquid assets. The forecasting model is built upon a feature set designed to capture the multi-faceted drivers of returns, spanning five domains: (i) **momentum**, (ii) **volatility**, (iii) **market microstructure**, (iv) **on-chain activity**, and (v) **cross-asset context**.

2.5 Methodology and Contributions

The central hypothesis is that the non-linear, interaction-heavy nature of this market demands a non-parametric approach. We propose an adapted **Quantile Regression Forests (QRF)** model (Meinshausen, 2006). QRF was selected as the primary model for several reasons. Firstly, its ensemble nature provides inherent robustness to the noisy predictors common in high-dimensional financial feature sets. Secondly, unlike gradient boosting, QRF's independent tree construction can be less prone to overfitting in non-stationary environments. Finally, its method of estimating quantiles from the full distribution of training samples in terminal nodes is a more direct and empirically stable approach than methods requiring separate models for each quantile. To tailor the model to a non-stationary financial time series, we apply: (i) **time-decay sample weights** to prioritise recent data; (ii) **non-crossing enforcement** via isotonic rearrangement across ; and (iii) **post-hoc calibration** using regime-aware residual-quantile offsets, with **split-conformal bands** as a robustness check. These adaptations are detailed in the Methodology 4.3–4 and Appendix 2.

Contributions.

1. **Methodology.** A QRF-based interval pipeline for 72-hour returns with time-decay weighting, isotonic non-crossing, and post-hoc calibration (residual-quantile; split-conformal as a check).
2. **Evaluation design.** Rolling, block-wise validation tailored to non-stationary crypto series; comparison to LQR and LightGBM using pinball loss, empirical coverage, and interval width.
3. **Empirical insight.** Feature-family analysis of tail drivers and an applied risk-use case (interval-aware sizing).

We benchmark our adapted QRF against a parametric **Linear Quantile Regression (LQR)** and a powerful **LightGBM** model (Ke *et al.*, 2017) augmented with **conformal prediction** (Romano, Patterson and Candès, 2019). Preliminary results suggest that the primary advantage of the adapted QRF framework lies in its superior ability to synthesise on-chain activity and market microstructure features to anticipate shifts in return distribution skewness—a dynamic that linear models fail to capture.

2.6 Scope and Delimitations

This dissertation provides a rigorous methodological and empirical analysis of interval forecasting. It does not aim to develop a complete, production-ready trading system, which would require further considerations such as transaction costs, liquidity constraints, and execution latency. Furthermore, the feature set, while comprehensive, is confined to publicly available market and on-chain data, thereby excluding alternative data sources such as social media sentiment or developer activity metrics, which may also contain predictive information. The findings are specific to the mid-cap tokens within the Solana ecosystem during the observation period and may not be directly generalisable to other blockchains, market-cap tiers, or market regimes without further investigation and potential recalibration.

2.7 Research Question

This framework motivates these core research questions:

1. **RQ1.** Do Quantile Regression Forests (QRF) deliver lower pinball loss for 72-hour returns than Linear Quantile Regression and LightGBM across $\{0.05, 0.10, 0.25, 0.50, 0.75, 0.90, 0.95\}$?
2. **RQ2.** After post-hoc calibration, do QRF intervals achieve closer-to-nominal coverage (80%/90%) with competitive width?
3. **RQ3.** Which feature families (momentum, volatility, liquidity, on-chain activity, cross-asset) drive tail behaviour in mid-cap Solana tokens?

3 Literature Review

3.0.1 The Challenge: Statistical Properties of Cryptocurrency Returns

The return distributions of cryptocurrencies are characterised by heavy tails, significant skew, and extreme kurtosis relative to traditional assets, reflecting the frequency of large, abrupt price movements (Gkillas and Katsiampa, 2018). This leptokurtosis is compounded by pronounced volatility clustering, periods of relative calm followed by explosive variability, a dynamic exacerbated by the market's continuous operation and fragmented liquidity, which can amplify shocks across uncoordinated venues.

Crucially, this extreme risk is also largely idiosyncratic to the crypto market. Major cryptocurrencies carry substantial tail risk that is not strongly correlated with traditional stock market indices; instead, extreme events are driven by crypto-specific factors such as investor sentiment, regulatory news, or network-level events (Borri, 2019). Furthermore, their returns show little to no exposure to standard macroeconomic risk factors, being influenced instead by internal drivers like network momentum and adoption metrics (Liu and Tsyvinski, 2021). This body of evidence demonstrates that classical financial risk models, with their reliance on Gaussian assumptions and traditional risk factors, are fundamentally misspecified for crypto assets. A credible forecasting framework must therefore abandon these assumptions and be built to incorporate the crypto-native features that drive risk.

3.1 Approaches to Quantile Estimation

Given the non-normal character of crypto returns established previously, estimating the full conditional distribution is more informative than forecasting its central tendency. Quantile regression provides a natural framework for this, but the choice between a restrictive parametric model and a flexible non-parametric one is critical.

3.1.0.1 The Parametric Benchmark: Linear Quantile Regression

Quantile regression, introduced by (Koenker and Bassett, 1978), generalises linear regression by estimating conditional quantiles directly. For a given quantile level $\tau \in (0, 1)$, the linear quantile regression (LQR) estimator solves:

$$\hat{\beta}_\tau = \arg\min_\beta \sum_{i=1}^{n} \rho_\tau(y_i - x_i^\top \beta)$$

where $\rho_\tau(u) = u(\tau - \mathbb{1}\{u < 0\})$ is the **pinball loss function**. While LQR provides a transparent and interpretable benchmark, its fundamental assumption of a fixed linear relationship across all quantiles represents a severe limitation. This rigidity is fundamentally at odds with the non-linear volatility dynamics and abrupt regime shifts that define cryptocurrency markets. Furthermore, the common practical issue of **quantile crossing**—where independently

estimated quantile lines intersect—can yield incoherent and unusable interval forecasts unless post-hoc remedies like rearrangement are applied (Chernozhukov, Fernández-Val and Galichon, 2010). These shortcomings do not merely motivate, but necessitate the exploration of more flexible, non-parametric methods.

3.1.0.2 Non-Parametric Solutions: Quantile Regression Forests

As a direct response to the limitations of linear models, Quantile Regression Forests (QRF), proposed by (Meinshausen, 2006), extend the Random Forest algorithm (Breiman, 2001) to estimate the entire conditional distribution. Instead of averaging outcomes in terminal nodes, QRF uses the full empirical distribution of training responses within the leaves to form a predictive distribution, from which conditional quantiles are derived.

This non-parametric approach is inherently well-suited to financial data; it naturally captures complex non-linearities and adapts to heteroskedasticity without pre-specification. However, QRF is not without its own challenges. Its theoretical foundation rests on an assumption of independent and identically distributed (i.i.d.) data—a condition clearly violated by financial time series. A naive application of QRF to time-ordered data can therefore lead to biased estimates. This violation is a central methodological challenge that requires specific adaptations, such as the time-decay weighting and rolling validation schemes discussed later, to apply the model soundly. Furthermore, the accuracy of its tail quantile estimates can degrade if the terminal leaves are sparsely populated, a genuine risk when modelling extreme events. Boosting offers another route to non-parametric quantile estimation, but with contrasting properties.

3.1.0.3 A Boosting Alternative: LightGBM for Quantiles

Gradient boosting presents another powerful non-parametric paradigm. It constructs an ensemble sequentially, with each new tree trained to correct the errors—specifically, the gradients of the loss function—of the preceding models (Friedman, 2001). This methodology can be directly applied to quantile regression by using the pinball loss as the objective. LightGBM (Ke *et al.*, 2017) is a highly efficient and scalable implementation of this idea, making it a formidable baseline.

In sharp contrast to QRF's parallelised construction, boosting's sequential focus on difficult-to-predict instances can yield sharper estimates in the tails. This potential for higher accuracy, however, comes with significant trade-offs. A separate model must typically be trained for each target quantile, imposing a considerable computational burden. The aggressive, error-focused fitting can also produce "ragged" and unstable quantile estimates in regions with sparse data and may overfit transient noise without careful regularisation. Finally, like LQR, independently fitted boosting models are susceptible to the problem of quantile crossing.

3.2 Ensuring Rigour: Calibration, Evaluation, and Comparison

Selecting a flexible forecasting model is insufficient on its own; its predictive performance must be evaluated using principled metrics, its outputs calibrated to ensure reliability, and its superiority over alternatives established through formal statistical tests.

3.2.0.1 Proper Scoring and Forecast Evaluation

A principled evaluation of probabilistic forecasts requires the use of **strictly proper scoring rules**, which incentivise the model to report its true belief about the future distribution. For quantile forecasts, the canonical proper scoring rule is the pinball loss (Gneiting and Raftery, 2007). As the metric being directly optimised by the models, it serves as the primary tool for evaluation. However, performance is not a single dimension. The quality of an interval forecast is judged by two distinct and often competing properties: **calibration**, the statistical consistency between the nominal coverage rate (e.g., 90%) and the empirical frequency of outcomes falling within the interval; and **sharpness**, the narrowness of the interval. An ideal forecast is one that is maximally sharp, subject to being well-calibrated. However, a model optimised on a proper score is not inherently guaranteed to be well-calibrated in finite samples. This gap between theoretical optimisation and empirical reliability motivates the use of formal calibration techniques.

3.2.0.2 Achieving "Honest" Intervals: Conformal Prediction

Conformal prediction provides a distribution-free framework to correct for such miscalibration. Specifically, Conformalized Quantile Regression (CQR) (Romano, Patterson and Candès, 2019) provides a mechanism to adjust a base model's quantile forecasts to achieve guaranteed marginal coverage. It uses a hold-out calibration set to compute a conformity score based on model errors, which is then used to adjust the width of future prediction intervals. While the underlying exchangeability assumption is violated in time series, employing a rolling calibration window of recent data provides a practical and widely used compromise to adapt the procedure to non-stationary environments.

3.2.0.3 Statistically Significant Comparisons: The Diebold-Mariano Test

To move beyond descriptive comparisons of average loss, formal statistical tests are required to determine if the performance difference between two models is significant. The **Diebold-Mariano (DM) test** (Diebold and Mariano, 1995) provides a standard framework for this, assessing the null hypothesis of equal predictive accuracy. The test statistic is given by:

$$DM = \frac{\bar{d}}{\sqrt{\hat{\mathrm{Var}}(\bar{d})}}$$

where $\bar{d}$ is the mean loss differential between two models. For the multi-step, overlapping forecasts used in this project, the sequence of loss differentials will be autocorrelated by construction. It is therefore critical to use a heteroskedasticity and autocorrelation consistent (HAC) variance estimator, as recommended by (West, 1996), to ensure valid statistical inference.

3.3 Methodological Requirements for Robust Time-Series Forecasting

The foundational literature establishes the potential of non-parametric models, but their successful application to volatile, non-stationary financial time series is contingent upon a number of specific methodological adaptations. This section reviews the literature concerning these essential requirements, from ensuring the logical coherence of predictions to adapting models to the temporal dynamics of the data.

3.3.0.1 Ensuring Coherent Predictions: Non-Crossing Quantiles

Models that estimate quantiles independently, such as LQR and standard gradient boosting, are susceptible to the critical failure of **quantile crossing**. This occurs when, for instance, a predicted 90th percentile falls below the predicted 50th percentile, yielding an illogically and unusable conditional distribution. To rectify this, (Chernozhukov, Fernández-Val and Galichon, 2010) proposed a post-processing "rearrangement" technique. This method applies isotonic regression to the initially estimated quantile function, projecting the unconstrained predictions onto the space of valid, non-decreasing distribution functions. This ensures the monotonicity of the quantile curve and is a critical step for producing valid prediction intervals.

3.3.0.2 Adapting to Non-Stationarity and Temporal Dependence

Financial time series are fundamentally non-stationary and autocorrelated, violating the i.i.d. assumption that underpins many machine learning models. Two distinct but related adaptations are required to address this.

First, to handle **non-stationarity** such as volatility clustering, the model must prioritise more recent information. The literature supports the use of **time-decay sample weights** to achieve this. (Taylor, 2008), for example, introduced exponentially weighted quantile regression for Value-at-Risk estimation, demonstrating that up-weighting recent observations yields more responsive and accurate tail forecasts in changing market conditions.

Second, to handle **temporal dependence**, model evaluation and hyperparameter tuning must respect the chronological order of the data. Standard k-fold cross-validation is invalid for time series, as it can lead to lookahead bias and produce misleadingly optimistic performance estimates. The literature therefore strongly advocates for rolling-origin or blocked cross-validation schemes, which preserve the temporal sequence by training only on past data to forecast the future, thereby simulating a live forecasting environment (Bergmeir, Hyndman and Koo, 2018).

3.3.0.3 Correcting for Bias and Ensuring Empirical Calibration

Even correctly specified quantile models can exhibit systematic biases in finite samples. As (Bai *et al.*, 2021) have shown, linear quantile regression can suffer from a theoretical **under-coverage bias**, where a nominal 90% interval may contain the true outcome significantly less than 90% of the time due to estimation error. This problem motivates the necessity of post-hoc calibration.

While the CQR framework discussed previously is one such solution, the literature offers several alternatives. Methods like the Jackknife+ (Barber *et al.*, 2021) and residual bootstraps provide different mechanisms for constructing prediction intervals with more reliable coverage properties. The existence of this rich literature on calibration highlights a crucial principle for risk management applications: a model's raw output cannot be taken at face value. An explicit calibration step is required to correct for inherent biases and ensure the resulting prediction intervals are empirically "honest".

3.4 Integrating Crypto-Native Data Sources

The literature on cryptocurrency risk factors makes it clear that models confined to historical price data are insufficient. The unique nature of blockchain-based assets provides a rich set of crypto-native data sources that are essential for capturing the specific drivers of risk and return in this asset class.

3.4.0.1 Market Microstructure and Liquidity

Like traditional markets, cryptocurrency price dynamics are influenced by liquidity and trading frictions. Empirical studies have documented that periods of market stress coincide with widening bid-ask spreads and evaporating order book depth (Dyhrberg, 2016). Furthermore, the on-chain nature of transactions introduces unique microstructural features, such as network congestion and transaction fees, which can impact market liquidity and price formation (Easley, O'Hara and Basu, 2019). Incorporating proxies for these effects is crucial, as it allows a model to dynamically adjust its estimate of uncertainty; for instance, by widening its prediction intervals in response to deteriorating market liquidity, thereby anticipating volatility spikes.

3.4.0.2 On-Chain Activity and Network Fundamentals

Blockchains provide a transparent ledger of network activity, offering powerful proxies for an asset's fundamental adoption and utility. Metrics such as the growth in active addresses, on-chain transaction counts, and, in the context of decentralised finance (DeFi), the Total Value Locked (TVL) in smart contracts, can signal shifts in investor sentiment and capital flows. Empirical studies consistently find that models augmented with on-chain metrics significantly outperform those based only on historical prices, as this data provides unique information about network health and demand (Sebastião and Godinho, 2021). These features allow a model to condition its forecasts on the fundamental state of the network, potentially informing not just the location but also the shape of the predictive distribution.

3.4.0.3 Cross-Asset Spillovers and Systemic Risk

The cryptocurrency market is a highly interconnected system where shocks to major assets like Bitcoin and Ethereum often propagate to smaller altcoins. This "connectedness" has been formally measured, showing significant return and, particularly, volatility spillovers from market leaders to the rest of the ecosystem (Diebold and Yilmaz, 2014; Koutmos, 2018). This implies that the risk of an individual token is not purely idiosyncratic; it is also a function of the broader crypto market's state. Consequently, any forecasting model that treats a token in isolation is fundamentally misspecified and is likely to underestimate systemic risk. A robust framework must therefore account for these cross-asset influences.

3.5 Synthesis and Conclusion

This review has established a clear and compelling justification for the methodology adopted in this dissertation. The unique statistical properties of cryptocurrency returns—heavy tails, volatility clustering, and dependence on idiosyncratic, on-chain factors—render traditional parametric models inadequate. This failure necessitates the use of flexible, non-parametric methods,

for which Quantile Regression Forests are a logical choice, given their ability to capture complex, non-linear relationships without restrictive distributional assumptions.

However, the literature also makes it clear that a naive application of any such model would be insufficient. A credible forecasting framework requires a series of specific, evidence-based adaptations. The need to adapt to non-stationarity justifies the use of time-decay weighting. The imperative for valid, coherent predictions necessitates post-processing to enforce non-crossing quantiles. The requirement for reliable out-of-sample evaluation mandates the use of rolling cross-validation. Finally, the well-documented tendency for quantile models to mis-calibrate compels the integration of a formal calibration step to ensure the final prediction intervals are empirically valid.

By synthesising these distinct strands of literature—from model selection to time-series adaptation and calibration—this project constructs an integrated and methodologically robust framework. This framework is specifically designed to address the multifaceted challenges of interval forecasting in the volatile and rapidly evolving cryptocurrency market.

4 Data and Features

The validity of any forecasting model is fundamentally constrained by the quality and integrity of its input data. For volatile and rapidly evolving assets like cryptocurrencies, constructing a robust, research-grade dataset is a critical prerequisite for meaningful analysis. This chapter details the multi-stage process undertaken to source, clean, and engineer the data used in this dissertation. It begins by defining the asset universe and data sources, then describes the construction of the target variable and the extensive feature engineering pipeline. Finally, it outlines the preprocessing steps taken to handle missing data and presents key insights from the exploratory data analysis that guided the modelling approach.

4.0.1 Data Sourcing and Asset Universe Definition

The foundation of this study is a bespoke, multi-source panel dataset constructed at a 12-hour resolution, specifically designed to support tail-sensitive, quantile-based forecasting. The data streams were aggregated from several high-quality APIs, using specific endpoints for different data types to ensure the highest fidelity for each signal.

The primary data sources included:

- **Price and Volume Data**: Historical Open-High-Low-Close (OHLC) and volume data for individual tokens were sourced from the **SolanaTracker API**, chosen for its deep liquidity and high-quality, reliable price feeds, which minimises the risk of spurious gaps or errors in the core price series.
- **On-Chain Metrics**: Key on-chain indicators for the Solana ecosystem, such as `holder_count` and `transfer_count`, were retrieved via the **CoinGecko API**, which provides broad coverage of token-specific network activity.
- **Global Context Data**: Broader market signals, including historical prices for Bitcoin (BTC) and Ethereum (ETH), as well as Solana-specific network metrics like transaction counts and Total Value Locked (TVL), were sourced from CoinGecko and the **Google BigQuery Solana Community Public Dataset**.

An initial effort was also made to incorporate social media sentiment data, given the narrative-driven nature of many Solana tokens. While an ingestion pipeline was successfully built, the data availability and quality were ultimately deemed insufficient for rigorous academic analysis and were excluded from the final feature set.

The **asset universe** was carefully defined from an initial, hand-picked list of 23 tokens based on their relevance to the Solana ecosystem. This list was then filtered according to a set of rigorous criteria. To be included in the final universe, a token had to satisfy:

- A **minimum market capitalisation** of $30 million to ensure a baseline of market significance and liquidity.
- A **minimum trading history** of six months. This was a crucial requirement to ensure a stable two-month (approx. 120 12-hour bars) training window was available for the initial backtest period for every asset in the universe.

This filtering was a deliberate and aggressive research design choice. Tokens with excessive missing data, insufficient history, or erratic reporting were pruned from the sample. This step is critical for quantile-based modelling, as tokens with inconsistent or late-starting data histories can inject significant bias into the empirical distribution, particularly distorting the tail estimates that are a primary focus of this research. By favouring data quality over sample size, this process ensures that the subsequent modelling results are attributable to the forecasting methodology itself, rather than being artefacts of poor-quality data.

The initial raw dataset comprised **8,326 rows across 23 tokens**. After applying the filtering criteria and cleaning procedures detailed in the following sections, the final asset universe for this study consists of **20 mid-cap Solana tokens**. The full dataset spans from **5th December 2024 to 3rd June 2025**, comprising a total of **6,464** 12-hour observations after cleaning and alignment.

4.0.2 3.2 Target Variable Construction and Properties

The predictive target for this study is the **72-hour forward-looking logarithmic return**, calculated at each 12-hour time step. It is formally defined as:

$$r_t^{(72h)} = \log(P_{t+6}) - \log(P_t)$$

where P_t is the closing price of the token at the end of the 12-hour bar at time t, and P_{t+6} is the closing price six 12-hour bars later. The use of logarithmic returns is standard practice in financial econometrics, as it provides a continuously compounded return that is time-additive and whose distribution more closely approximates normality than simple returns.

The combination of a **12-hour data cadence** and a **72-hour forecast horizon** was a deliberate design choice to create a target variable suitable for mid-frequency trading strategies. The 12-hour aggregation smooths the extreme noise present in sub-hourly price changes, while the 72-hour horizon is long enough to capture significant, economically meaningful moves where tail events and distributional properties become highly relevant. This choice aims to maximise the signal-to-noise ratio for the specific purpose of forecasting the distribution of multi-day returns.

Exploratory analysis confirms that the resulting target variable exhibits the extreme non-normal characteristics that motivate this research. As shown in **Table 3.1**, the pooled distribution of 72-hour log returns is highly leptokurtic and positively skewed. With a **kurtosis of 20.73**, it demonstrates exceptionally fat tails compared to a normal distribution (kurtosis of 3), indicating that extreme price movements are far more common than a Gaussian model would suggest.

Statistic	Value
Mean	0.0031
Standard Deviation	0.1259
Skewness	**1.68**
Kurtosis	**20.73**
Minimum	-0.75
Maximum	1.02

Table 3.1: Summary Statistics for the 72-hour Log Return Target Variable (Pooled Across All Tokens).

The heavy-tailed nature of the target is further illustrated in **Figure 3.1**, which plots the empirical distribution against a normal distribution with the same mean and variance. The substantially higher peak and elongated tails of the empirical distribution provide clear visual evidence that a Gaussian assumption would be inappropriate and underscore the necessity of a quantile-based modelling approach.

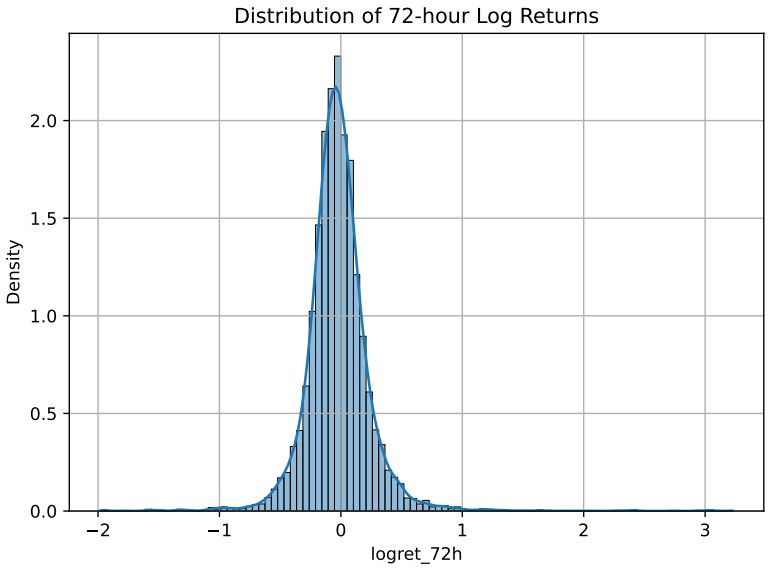

Figure 4.1: Distribution of the 72-hour log return target variable, pooled across all tokens. The distribution exhibits a sharp peak and significantly heavier tails than a comparable normal distribution, justifying the use of quantile-based models.

Furthermore, the properties of this distribution are not static. Analysis of the underlying 12-hour returns reveals that the shape of the distribution is highly conditional on the broader market environment. By defining macro-regimes based on the quartiles of SOL's 12-hour return, it becomes evident that the conditional distribution of token returns shifts systematically. As shown in **Figure 3.2**, "Bull" regimes are associated with positive skew and a fatter right tail, whereas "Bear" regimes exhibit heavier left tails, signalling increased downside risk. This empirical finding of **regime-dependence** is critical, as it justifies the need for a *conditional* forecasting model that can adapt its predicted quantiles based on contextual features.

Finally, it is important to note that this construction results in an **overlapping target variable**. A new 72-hour forecast is generated every 12 hours, meaning that the forecast periods overlap significantly. This has direct implications for the evaluation methodology, as the resulting forecast errors will be serially correlated by construction. As detailed in the literature review and methodology chapters, this requires the use of specific techniques, such as blocked cross-validation and HAC-robust statistical tests, to ensure valid inference.

4.0.3 Data Preprocessing and Cleaning

Before any features could be engineered, the raw, multi-source panel dataset underwent a rigorous cleaning and preprocessing pipeline. This was a critical phase designed to handle the significant data quality challenges inherent in cryptocurrency markets, such as missing observations and inconsistent token histories, ensuring the final dataset was robust and suitable for modelling. The initial raw data contained approximately **18% missing values** in the core OHLCV columns alone, with some on-chain features like `holder_count` missing nearly 40% of their data (see Appendix **Table @tbl:apx-missing-top10** for a full breakdown).

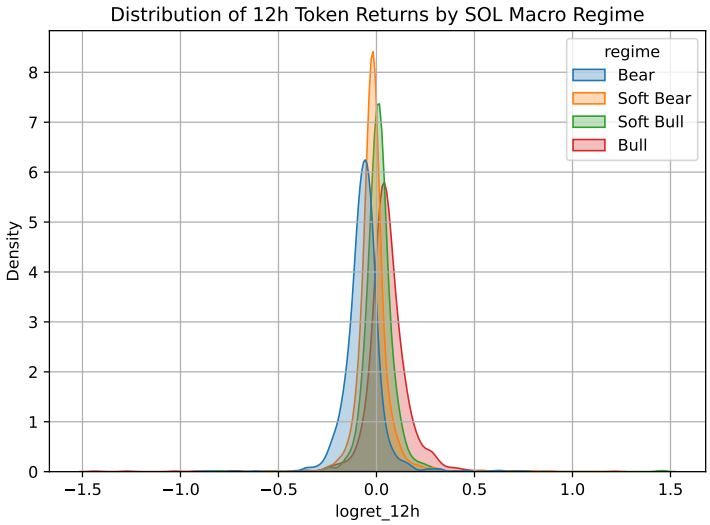

Figure 4.2: Conditional distribution of 12-hour token returns, faceted by the SOL macro-regime. The shape, skew, and tail behaviour of the returns change significantly depending on the broader market context.

The nature of this missingness was not uniform. As illustrated by the heatmap in **Figure 3.4**, the data gaps were highly structured. Some tokens (e.g., `MEW`, `ZEREBRO`) had clean data but only after a late start date, while others exhibited intermittent, patchy gaps throughout their history. This heterogeneity necessitated a multi-step strategy rather than a single, one-size-fits-all approach.

Figure 3.4: *Heatmap of OHLCV data presence across the token universe over time (Green = Present, Red = Missing). The block-like structure for some tokens indicates late listings, while sporadic red patches show intermittent data gaps, motivating a hybrid cleaning strategy.*

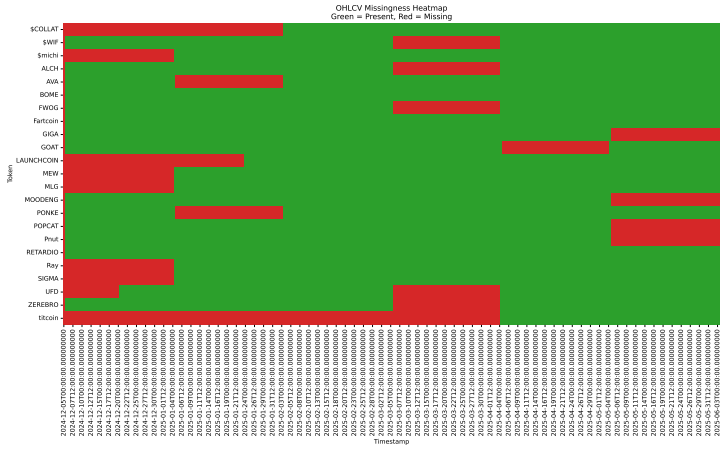

Figure 4.3: Heatmap of OHLCV data presence across the token universe over time (Green = Present, Red = Missing). The block-like structure for some tokens indicates late listings, while sporadic red patches show intermittent data gaps, motivating a hybrid cleaning strategy.

4.0.3.1 Temporal Alignment and Clipping

To ensure temporal consistency, each time series was first clipped to begin only from its first fully valid OHLCV observation. This step, detailed in the strategy summary in Appendix **@sec-cleaning-strategy**, removes spurious data from pre-launch or illiquid initial listing periods, which could otherwise contaminate the analysis. Tokens with insufficient history after this clipping process (e.g., `$COLLAT`) were dropped from the universe entirely.

4.0.3.2 Imputation Strategy

A key challenge was to fill the remaining intermittent gaps without distorting the underlying distributional properties of the data. Several imputation methods were benchmarked on simulated missing data. Counter-intuitively, the analysis revealed that a simple **linear interpolation** outperformed more complex methods like Kalman smoothing in terms of Root Mean Squared Error (RMSE) (see Appendix **@#imp-table** for benchmark results). This finding suggests that for small, sporadic gaps, a simple interpolation preserves the local price trajectory and its inherent noise structure more effectively than methods that impose stronger, potentially smoothing, structural assumptions.

Therefore, the final strategy adopted was a hybrid approach: **linear interpolation** to fill the majority of gaps, supplemented by a **forward-fill** for a maximum of two consecutive 12-hour bars.

4.0.3.3 Imputation-Awareness

Crucially, the imputation process was not treated as a silent correction. For every feature that was imputed, a corresponding binary **imputation mask** variable was created. This flag takes a value of `1` if the original data point at that timestamp was missing and subsequently imputed, and `0` otherwise. This technique of "imputation-awareness" is a key methodological choice, as it allows the machine learning model to learn directly from the patterns of missingness. This is particularly relevant in crypto markets, where data gaps themselves can be a predictive signal (e.g., indicating an exchange API outage or a period of extreme market stress).

4.0.4 Exploratory Data Analysis

Following the preprocessing pipeline, an extensive exploratory data analysis (EDA) was conducted to uncover the key empirical properties of the data. This section presents the three most critical findings that provide a direct, data-driven justification for the subsequent feature engineering choices and the selection of a non-parametric, conditional forecasting model.

4.0.4.1 Volatility Clustering and Asymmetric Leverage

The data exhibits two foundational properties of financial time series that invalidate simple, static risk models. First, strong **volatility clustering** is evident in the autocorrelation of absolute 12-hour returns, confirming that risk is time-varying and motivating the inclusion of dynamic volatility features.

Second, the relationship between returns and subsequent volatility is asymmetric. An analysis regressing 12-hour log returns against forward 36-hour realised volatility reveals a distinct U-shaped pattern, as shown in **Figure 3.5**. This confirms that variance is conditional on the

magnitude of recent returns, with large moves in either direction predicting elevated future volatility. The effect is slightly stronger for negative returns, consistent with a "crypto leverage effect" where downside shocks lead to greater market instability. This non-linear dynamic necessitates a modelling approach, such as the Quantile Regression Forest used in this study, that can naturally capture such relationships and adapt its prediction interval widths based on the direction and magnitude of recent price shocks.

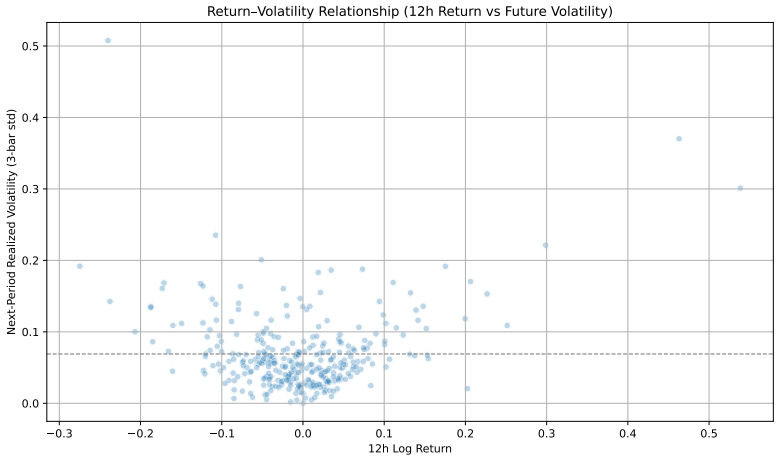

Figure 4.4: A scatter plot of 12h Log Return vs. Next-Period Realised Volatility. The U-shaped pattern, with a slightly steeper slope for negative returns, illustrates the asymmetric leverage effect.

4.0.4.2 Feature Redundancy and Collinearity

An analysis of the correlation structure between 18 core features was conducted to identify potential multicollinearity, which can destabilise tree-based ensemble models. As shown in the Pearson correlation matrix in **Figure 3.6**, several feature pairs exhibit extremely high linear relationships. The most significant correlations were observed between:

- `token_close_usd` and `token_volume_usd` (r $approx 0.999$)
- `btc_close_usd` and `tvl_usd` (r $approx 0.94$)
- `sol_close_usd` and `tvl_usd` (r $approx 0.89$)

This finding is critical. While these raw fields were retained for the initial feature engineering phase to allow for the construction of richer indicators (e.g., from OHLC data), this analysis motivates the necessity of a subsequent feature pruning step. Reducing this high level of collinearity before modelling is essential for improving the stability, training speed, and interpretability of the final Quantile Regression Forest.

4.0.4.3 The Empirical Failure of Gaussian Assumptions

To provide a definitive, data-driven justification for model selection, a baseline experiment was conducted to compare a naive Gaussian interval forecast (defined as
pmz
$cdot$

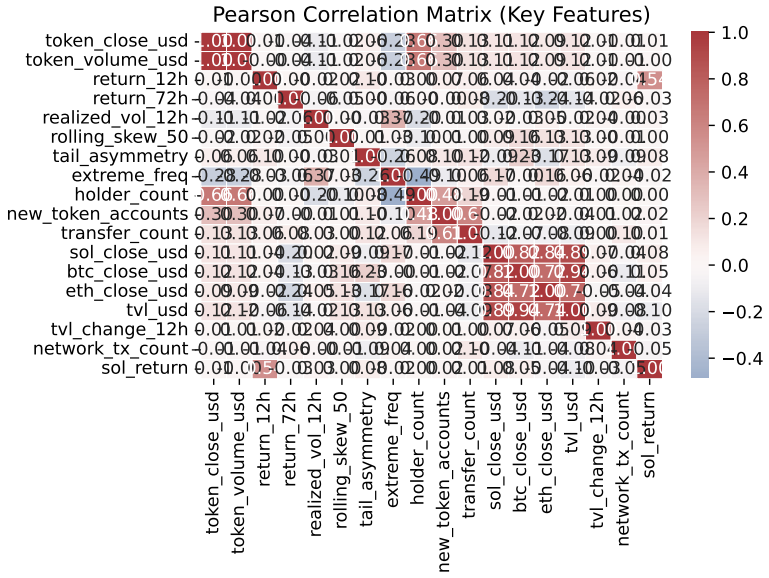

Figure 4.5: Pearson correlation matrix of key features. The strong red blocks highlight pairs of highly correlated variables, necessitating a feature pruning or aggregation strategy.

sigma, using realised volatility) against a simple Quantile Regression Forest. The results, shown in **Figure 3.7**, are stark.

The naive Gaussian intervals systematically **under-cover** the true outcomes across all nominal levels; for example, a nominal 80% interval achieves only ~70% empirical coverage. In contrast, even a basic QRF model tracks the ideal 45-degree line far more closely, demonstrating superior **calibration** by adapting to the true fat-tailed and skewed nature of the returns.

Crucially, this improvement in calibration does not come at the cost of precision. At a nominal 80% coverage level, the QRF intervals were also significantly **sharper**, with an average width of 0.1682 compared to 0.2038 for the naive method. This dual failure of the Gaussian approach—in both calibration and sharpness—provides the ultimate empirical justification for rejecting simple parametric assumptions and adopting a non-parametric methodology like QRF for this dataset.

4.0.5 3.5 Feature Engineering and Selection

Following the data preparation and exploratory analysis, an extensive feature set was engineered. This process was guided by two main principles: first, all predictors must be strictly causal, using only information available at or before time t; second, the feature set should be designed to capture the specific statistical properties—such as volatility clustering, asymmetry, and regime-dependence—identified in the EDA.

4.0.5.1 3.5.1 Feature Construction by Family

The engineered set focuses on signals that respond to the unique dynamics of cryptocurrency markets. The literature supports using a diverse set of technical and on-chain indicators, as machine learning models can effectively synthesise these signals to improve predictive accuracy `[@Akyildirim2021]`. The constructed features fall into five families:

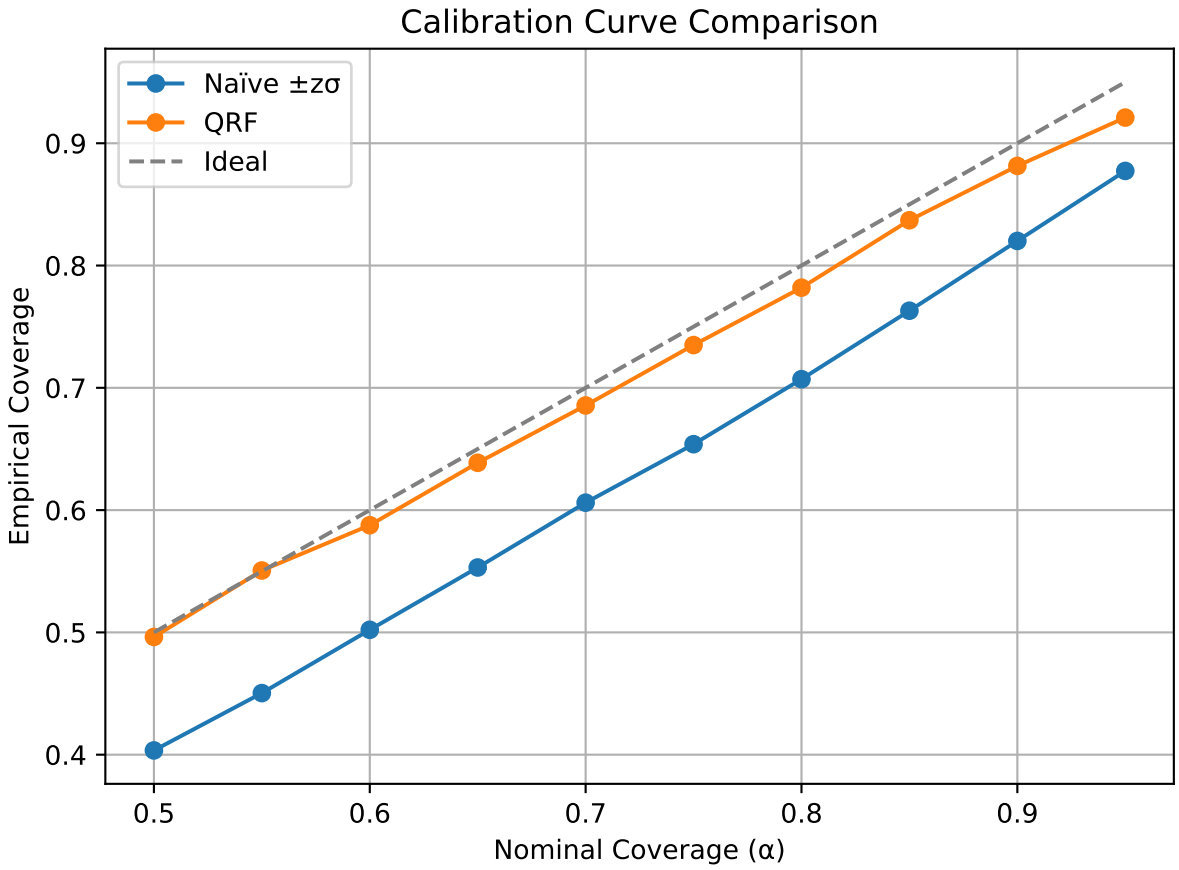

Figure 4.6: Calibration curve comparing the empirical vs. nominal coverage of naive Gaussian intervals and QRF intervals. The QRF's proximity to the ideal line demonstrates its superior ability to model the data's true distribution.

1. **Momentum & Trend:** Standard indicators such as 12h and 36h log-returns, the 14-period Relative Strength Index (RSI), and MACD were created to capture trend and mean-reversion dynamics.
2. **Volatility & Tails:** To model the observed volatility clustering and leverage effects, features such as realised volatility over 3 and 6 bars, downside-only volatility, and the Average True Range (ATR) were included. Higher-moment estimators like rolling 36-hour skewness were also engineered to capture tail asymmetry.
3. **Liquidity & Flow:** The Amihud illiquidity measure and volume z-scores were constructed to provide the model with signals about market depth and trading frictions, which are conditions under which prediction intervals should widen.
4. **On-Chain Activity:** To capture fundamental network health, features such as the growth rate of unique wallets and the ratio of new accounts to total holders were included, consistent with the on-chain data availability constraints.
5. **Market Context:** To model the cross-asset spillovers identified in the literature, features such as the 12h returns for SOL, BTC, and ETH, as well as the rolling 36h correlation of each token to these majors, were created. This explicitly allows the model to learn a dynamic, implicit beta to the broader market.

A complete feature dictionary, including formulas and window lengths, is provided in Appendix [Appendix ID].

4.0.5.2 3.5.2 Redundancy Control and Pruning

The initial engineering process generated over 90 candidate features. To create a final feature set that was both predictive and robust, a systematic, three-stage pruning pipeline was implemented:

1. **Initial Filtering:** Features with near-zero variance or excessive missingness (>80%) were removed.
2. **Collinearity Filter:** To improve model stability, one feature from any pair with a Pearson correlation coefficient $|\rho| > 0.98$ was removed.
3. **Gain-Based Pruning:** A computationally inexpensive LightGBM model was trained to predict the median ($\tau = 0.50$) return. Any feature contributing less than 0.3% to the total gain was pruned. This resulted in a core set of **29 predictors** that explained **99.3%** of the model's total gain.

The resulting feature set, designated `features_v1`, was frozen for all subsequent median-based modelling. A second set, `features_v1_tail`, was created by reintroducing several theoretically important but low-gain tail-risk indicators (e.g., `extreme_count_72h`) for use in the final quantile models. This structured process ensures the models are built upon a rich, yet parsimonious, set of predictors.

5 Methods

This section formalises the modelling and evaluation frame used throughout the dissertation. It defines the target, records leakage controls, and specifies the rolling train–calibrate–test design under which all models are compared. **Notation and symbols follow Appendix @ref(app-m0-notation).**

Objective and target. For each token i at decision time t (12-hour cadence), we forecast conditional quantiles of the **72-hour** log return

$$y_{i,t+6} = \log C_{i,t+6} - \log C_{i,t},$$

where $C_{i,t}$ denotes the 12-hour close. At quantile level $\tau \in (0,1)$, we learn predictors $\hat{q}_\tau(x)$ using the **pinball loss** (see Appendix M1; Koenker & Bassett, 1978; Koenker, 2005).

Panel scope and pooling. Models are trained **per token** (no cross-sectional pooling). Within each rolling window, token i's model uses only its own history. The design matrix is the pruned **feature-set v1 (29 predictors)** defined in §3, including categorical dummies where applicable.

Rolling evaluation protocol. For each token we use a blocked walk-forward design:

$$\text{Train} = 120 \text{ bars } (\approx 60 \text{ d}) \;\Rightarrow\; \text{Calibration} = 24 \text{ bars} \;\Rightarrow\; \text{Test} = 6 \text{ bars } (72 \text{ h}),$$

advanced by **step = 6 bars** so that tests are non-overlapping. *PLACEHOLDER — Figure:* `(@fig-rolling)` Rolling scheme diagram (Train→Cal→Test, step = 6).

Calibration and non-crossing. Base quantiles are made **monotone in** τ via row-wise **isotonic rearrangement** (pool-adjacent-violators), then **central bands** are adjusted using **split-conformal prediction** (citations as above). Formal score definitions and the order-statistic inflation used for 80 % and 90 % bands are given in **Appendix M2** (see also listings `A-isotonic.py` and `A-conformal.py`).

Models and libraries. - **LQR:** linear quantile regression via `statsmodels.QuantReg`. - **LightGBM:** gradient-boosted trees with quantile objective per τ. - **QRF:** Quantile Regression Forests; one shared forest predicts all τ. Full software and environment details are reported in **Appendix R1** (`@tbl-software`).

5.1 Linear Quantile Regression (Baseline) Model

For each $\tau \in \{0.05, 0.10, 0.25, 0.50, 0.75, 0.90, 0.95\}$ and token i, we fit an independent **Linear Quantile Regression** model that minimises the check (pinball) loss to estimate $\hat{q}_\tau(x)$ (Koenker & Bassett, 1978; Koenker, 2005). The formal program is given in **Appendix (?)(app-l1-lqr)**.

Design matrix and preprocessing. We use the pruned **feature-set v1 (29 predictors)** (§3). Numerical columns are **standardised on the Train slice only**; categorical indicators (e.g., day-of-week) are **one-hot** with an intercept. No additional within-pipeline transforms are applied.

Estimation. Models are fit with `statsmodels.QuantReg`; implementation notes (solver and tolerances) appear in **Appendix (?)(app-r2-lqr-impl)**. There are no tree/boost hyperparameters; effective complexity is governed by the design matrix. Convergence was stable across rolling slices.

Non-crossing and calibration. Because per-τ fits can cross, we enforce **monotonicity in τ** via row-wise **isotonic rearrangement**; details in **Appendix (?)(app-m1-isotonic)**. Central prediction bands are then **split-conformally** adjusted; score definitions and order-statistic inflation are in **Appendix (?)(app-m2-conformal)**.

Rolling protocol. Evaluation follows the **Train 120 → Cal 24 → Test 6** scheme with **step = 6** (non-overlapping Test windows) defined in §4.1.

Reporting. We present **pinball loss** by τ, **calibration curves** and **coverage/width** at 80 %/90 %, and **Diebold–Mariano** tests vs. LightGBM and QRF (test specification in §4.5 and **Appendix (?)(app-m4-tests)**).

Figures and appendix cross-references. *Main text:* compact **LQR calibration** panel and a small **pinball-by-τ** table. *PLACEHOLDER — Figure:* `(@fig-lqr-calib)` LQR calibration curve (Test). *PLACEHOLDER — Table:* `(@tbl-lqr-pinball)` Pinball loss by quantile (Test). *Appendix:* per-token **fan charts** and **coverage-by-token** bars; code listings. *PLACEHOLDER — Listings:* `A-LQR-fit.py` (fit & preprocessing), `A-conformal.py` (bands).

Why this baseline. LQR provides a transparent **parametric** benchmark. In heavy-tailed, skewed crypto returns, its characteristic **tail mis-calibration** (cf. `@fig-lqr-calib`) motivates the flexible, non-parametric models in §§4.3–4.4.

5.2 4.3 Gradient-boosted trees with quantile loss (LightGBM baseline)

Model (summary). For each $\tau \in \{0.05, 0.10, 0.25, 0.50, 0.75, 0.90, 0.95\}$ and token, we fit an independent **LightGBM** regressor with the **quantile (pinball) objective**, yielding $\hat{q}_\tau(x)$ (Koenker & Bassett, 1978; Ke et al., 2017). Formal boosting and gradient expressions appear in **Appendix (?)(app-g1-lgbm-obj)**.

Design matrix & preprocessing. We use the pruned **feature-set v1 (29 predictors)** (§3). Numerics are **not scaled**; categoricals (e.g., `day_of_week`) are supplied via LightGBM's native categorical handling (or one-hot where required). No monotone constraints are imposed. Determinism is enforced via fixed seeds and `deterministic=True`.

Variant and final choice. Earlier variants trained a single **point** model and formed residual-based intervals. The **final baseline** trains **per-quantile** models and conformalises only the **central band** $[\hat{q}_{0.10}, \hat{q}_{0.90}]$; the procedure is summarised below and detailed in **Appendix (?)(app-m2-conformal)**. This specification calibrated more reliably under regime shifts than residual intervals.

Non-crossing and calibration. Because per-τ models are independent, we enforce monotonicity $\hat{q}_{0.05} \le \cdots \le \hat{q}_{0.95}$ via row-wise **isotonic rearrangement** (Appendix (?)(app-m1-isotonic)). The 80 % and 90 % central bands are then **split-conformally** adjusted using two-sided scores

on the 24-bar calibration slice (Appendix (**?**)(app-m2-conformal)); a small one-sided tail tweak is applied only at 0.05/0.95.

Rolling protocol & early stopping. Per token we use **Train 120 → Cal 24 → Test 6** with **step = 6** (§4.1). **Early stopping** monitors pinball loss on the calibration slice; hyper-parameters are tuned once in a global Optuna study and then **fixed** for evaluation.

Reporting. We present **pinball loss** by τ, **calibration curves** and **coverage/width** at 80 %/90 %, and **Diebold–Mariano** tests vs. LQR and QRF (specification in §4.5; formulas/code in Appendix (**?**)(app-m4-tests)).

Figures / tables (Methods-appropriate). *Main text:* one compact **LightGBM calibration** panel; optionally a 1-row **pinball-by-τ** table. *PLACEHOLDER — Figure:* `(@fig-lgbm-calib)` Calibration curve (Test, post split-conformal). *PLACEHOLDER — Table:* `(@tbl-lgbm-pinball)` Mean pinball loss by quantile. *Appendix:* per-token **fan charts**, **coverage-by-token** bars, and the **hyper-parameter table**. *PLACEHOLDER — Appendix table:* `(@tbl-lgbm-hparams)` Final quantile hyper-parameters by τ. *PLACEHOLDER — Listings:* `A-LGBM-train.py` (fit), `A-conformal.py` (bands), `A-isotonic.py` (non-crossing).

Why this baseline. Quantile LightGBM is a strong, non-linear comparator that is fast, interaction-aware, and—after split-conformalisation—near-nominal in coverage with comparatively tight bands, setting a demanding reference for QRF (§4.4).

5.3 4.4 Quantile Regression Forests (core model)

Rationale. Random-forest quantile regression estimates conditional quantiles **without** parametric distributional assumptions and is robust to skew, heavy tails, and high-order interactions (Meinshausen, 2006). Unlike per-τ boosted trees, a **single forest** supplies all requested quantiles from a shared leaf-wise conditional distribution, improving stability—especially in the tails.

5.3.1 4.4.1 Estimator (summary)

We use a single forest to obtain $\{\hat{q}_\tau(x)\}$ by reading quantiles from the leaf-level conditional distribution at prediction time. In our implementation, **time-decay sample weights** enter both split selection and the leaf distributions. The full weight construction and the exact weighted-quantile estimator are provided in **Appendix (?)(app-m3-qrf)** (with equations).

5.3.2 4.4.2 Implementation

Library. `quantile-forest` (`RandomForestQuantileRegressor`), returning $\{\hat{q}_\tau\}$ for any grid via `predict(..., quantiles=[...])`.

Final specification (fixed across folds). `n_estimators = 1050`, `max_depth = 26`, `min_samples_leaf = 6`, `max_features = 0.98`, `bootstrap = True`, `n_jobs = -1`, `random_state = 42`, `sample_weight` = exponential **time-decay** (half-life **60 bars**; see §4.4.3).

Tuning. Hyper-parameters were selected once via a **global Optuna** study (objective: mean pinball loss averaged over τ and folds) and then **fixed** for all rolling evaluations. *PLACEHOLDER — Appendix table:* `(@tbl-qrf-hparams)` Hyper-parameters, search ranges, and best values. *PLACEHOLDER — Appendix listing:* `A-QRF-fit.py` (training pipeline and seeds).

Design matrix. Common **feature-set v1** (§3); numerics unscaled; categoricals one-hot in the preprocessing step.

5.3.3 4.4.3 Recency weighting (time-decay)

To reflect regime drift, each training observation at relative age Δt bars is exponentially down-weighted (half-life **60 bars**); the normalised weights sum to one. The exact form used in code appears in **Appendix (?)(app-m3-qrf)** (and helper `compute_decay_weights` in `A-helpers.py`).

5.3.4 4.4.4 Non-crossing and calibration (summary)

Monotone quantiles. Because quantiles are computed independently on the shared forest, we enforce monotonicity in τ via row-wise **isotonic rearrangement**; details in **Appendix (?)(app-m1-isotonic)**.

Residual-quantile calibration (RQC). On the **24-bar calibration** slice, we compute residuals against rearranged base quantiles and apply **regime-aware** (quiet/mid/volatile) residual-quantile offsets with mild winsorisation and an imputation filter. Procedure and formulas in **Appendix (?)(app-m2-conformal)** (RQC section).

Split-conformal bands (robustness). As a robustness check, we also form **split-conformal** central bands via two-sided scores on the calibration slice; score and order-statistic definitions are in **Appendix (?)(app-m2-conformal)**.

5.3.5 4.4.5 Computational choices and limitations

- **Honesty/OOB.** No "honest" splitting; out-of-bag predictions used only for diagnostics.
- **Leaf mass and depth.** Deep trees (`max_depth` = 26) capture non-linearities but can thin leaves; `min_samples_leaf` = 6 maintains stability for tail quantiles.
- **Shared forest.** One forest serves all τ, reducing per-τ variability and easing non-crossing enforcement.

5.3.6 4.4.6 Reporting and artefacts

We report **pinball loss** at each τ; **calibration curves** (empirical $\widehat{F}_\tau$ vs nominal τ); **coverage/width** for 80 %/90 % bands; and **Diebold–Mariano** comparisons vs LQR and LightGBM (spec §4.5; implementation in **Appendix (?)(app-m4-tests)**). Prediction CSVs and per-fold losses are archived. *PLACEHOLDER — Appendix folder:* `A-Artifacts/` (per-fold `*_preds.csv`, `*_pinball.csv`).

Figures / tables (Methods-appropriate). *Main text:* one **QRF fan chart** (representative token) and one **QRF calibration** panel. *PLACEHOLDER — Figure:* `(@fig-qrf-fan)` Fan chart (72-h bands, representative token). *PLACEHOLDER — Figure:* `(@fig-qrf-calib)` Calibration curve (Test). *Appendix:* coverage-by-token bars; extended fans; residual-offset diagnostics; **QRF hyper-parameter** table (`@tbl-qrf-hparams`).

Why QRF as the core model. Heavy-tailed, skewed returns with interaction-rich predictors favour a non-parametric distribution estimator. The shared-forest quantile extraction, coupled with simple regime-aware residual calibration, delivered **well-calibrated** and **sharp** intervals in rolling tests while remaining transparent and reproducible.

5.4 4.5 Validation, metrics, and statistical tests

This section formalises the rolling evaluation and the criteria used to compare models; full notation and conventions follow **Appendix (?)(app-m0-notation)**.

5.4.1 4.5.1 Rolling evaluation design

All models are evaluated **per token** via a blocked, walk-forward procedure with **non-overlapping** Test windows:

- **Train** = 120 bars (~60 d) → **Calibrate** = 24 bars → **Test** = 6 bars (72 h),
- **Step** = 6 bars (adjacent Tests do not overlap),
- Features at time t use only information available by the close of bar t (§3); the target is y_{t+6}.

Fit occurs on **Train** only; **non-crossing** (isotonic) and **calibration** (split-conformal or residual-quantile offsets) use **Cal** only. Performance is recorded on **Test** (strictly out-of-sample). We report both **micro** and **macro** averages across tokens; precise formulas and the rolling schematic are in **Appendix (?)(app-m0-notation)** (Fig. `@fig-rolling`).

5.4.2 4.5.2 Losses and calibration metrics

- **Pinball (check) loss.** Primary score for each τ; see definition in **Appendix (?)(app-m1-pinball)**. We report per-τ means (dispersion across tokens/folds) and a composite average over $\mathcal{T} = \{0.05, 0.10, 0.25, 0.50, 0.75, 0.90, 0.95\}$.
- **Empirical coverage & average width.** For central $(1-\alpha)$ bands (after non-crossing + calibration) we report coverage, average width, **coverage error** $|\widehat{\mathrm{cov}} - (1-\alpha)|$, and **conditional coverage** by predicted-width deciles. Exact formulas appear in **Appendix (?)(app-m5-metrics)**.
- **Quantile reliability / calibration curves.** We plot empirical hit-rates $\widehat{F}_\tau$ against nominal τ; perfect calibration lies on the 45° line. Formal definition is in **Appendix (?)(app-m5-metrics)**.
- **Optional proper scoring rule.** We compute the **interval score** (Gneiting & Raftery, 2007) for completeness; see **Appendix (?)(app-m5-metrics)**. (CRPS links are noted there.)

A summary of metrics and reporting conventions appears in **Table `@tbl-metrics-defs` (Appendix)**.

5.4.3 4.5.3 Statistical comparisons

Pairwise comparisons use **Diebold–Mariano** tests on loss differentials with **Newey–West** HAC variance and the **Harvey–Leybourne–Newbold** small-sample correction. We conduct **two-sided** tests and control multiplicity across τ using **Benjamini–Hochberg** FDR at $q = 0.10$ (Holm–Bonferroni reported as strict bounds). Full formulas, HAC settings, and code are provided in **Appendix (?)(app-m4-tests)** and listing `A-DM-HAC.py`.

5.4.4 4.5.4 Placement of figures and tables (handoff to Results)

Main text (limit to 3–4 items):

- **Calibration curves** (one panel per model): `@fig-lqr-calib`, `@fig-lgbm-calib`, `@fig-qrf-calib`.
- **Mean pinball loss by** τ (compact table): `@tbl-pinball-by-tau`.
- **Representative fan chart** (72-h band adaptivity): `@fig-fan-repr`.
- **Coverage/width** summary (80%/90%): `@tbl-cov-width`.

Appendix (diagnostics & reproducibility): Coverage-by-token bars, extended fan charts, pinball dispersion across folds, and **DM test** tables (with HAC lag and HLN factor). Listings for calibration, rearrangement, tests, and the environment file: `A-conformal.py`, `A-isotonic.py`, `A-DM-HAC.py`, `A-env.txt`.

6 5. Results

6.1 Experimental setup

We evaluate **LQR**, **LightGBM-Quantile**, and **QRF** on the rolling **Train 120 → Cal 24 → Test 6** design (step = 6; non-overlapping Tests), across the -grid $\{0.05, 0.10, 0.25, 0.50, 0.75, 0.90, 0.95\}$. Unless noted otherwise, results are **micro-averaged** across all test observations (with **macro** averages by token in parentheses). We report **pinball loss** (Table `@tbl-pinball-tau`), **coverage and width** of 80%/90% bands (Table `@tbl-cov-width`), **reliability curves** (Fig. `@fig-reliability-global`), and **width distributions** (Fig. `@fig-widths`). Pairwise significance is assessed later via **DM–HAC (HLN-adjusted)** (§5.3).

For supporting Plots and Tables follow Appendix @ref(app-r1).

6.2 Overall accuracy and calibration

Across the pooled rolling evaluation, **QRF** delivers the **lowest mean pinball loss at the left tail and lower-middle quantiles** ({0.05, 0.10, 0.25}), remains **competitive around the median**, and tracks the upper tails closely. **LightGBM** is generally less accurate (higher pinball) but attains **high coverage by producing wider intervals**. **LQR** is competitive near the centre and upper quantiles but **systematically under-covers**. In terms of calibration, **QRF's 90% bands are close to nominal** (0.87–0.89), while **80% bands remain modestly under-covered** (0.76–0.78). LightGBM **over-covers** (e.g., ~0.98–0.99 at 90%), consistent with conservative widths. These patterns hold at both the pooled (micro) level and when averaging per token (macro).

6.2.1 Pinball accuracy by quantile

?@tbl-pinball-tau reports the **mean pinball loss by tau and model** (standard errors in parentheses; micro and macro reported). The main findings are: | | LQR | LightGBM | QRF | |:—|:——-|:———|:——-| | 0.05 | 0.03015| 0.03514 | 0.01406| | 0.10 | 0.04094| 0.03108 | 0.02244| | 0.25 | 0.05524| 0.04556 | 0.04159| | 0.50 | 0.06302| 0.06581 | 0.06103| | 0.75 | 0.05539| 0.07374 | 0.07162| | 0.90 | 0.03707| 0.06622 | 0.06597| | 0.95 | 0.02399| 0.05957 | 0.04783|

- **Lower tail (= 0.05, 0.10):** QRF attains the lowest loss, with a sizable margin over LightGBM and a clear advantage over LQR. This indicates **superior tail sensitivity**—crucial in heavy-tailed return series.
- **Lower-middle (= 0.25):** QRF remains best. This is the region where models often drift if lower-tail calibration is imperfect; the improvement reflects the corrected residual-offset rule (see below).
- **Centre/upper (= 0.50, 0.75, 0.90, 0.95):** LQR is competitive to slightly better at the strict median and some upper on **pinball** (a linear model can approximate the median well on smoothed features), but QRF is **close** and often within the standard error; LightGBM typically has the **largest loss**.

- The **rank ordering** corresponds to the bar chart in Fig. **?@fig-reliability-global** (QRF's line adheres tightly to the 45° band except for a mild 80% under-coverage discussed below) and your pinball bar plot (QRF best at 0.05–0.25; LQR competitive around 0.50–0.95; LightGBM worst across).

Interpretation. QRF's non-parametric trees capture non-linear interactions that matter most in the **tails and asymmetric regimes**; LQR's linear structure can excel near the centre when the conditional median depends smoothly on features. LightGBM's comparatively higher pinball reflects a tendency to produce **over-conservative intervals** after calibration.

6.2.2 5.2 Overall accuracy and calibration

6.2.2.1 Global calibration and reliability

Figure **?@fig-reliability-global** plots the **reliability curve**—the empirical hit-rate $\Pr\{y \leq \hat{q}_\tau\}$ against the nominal τ—with Wilson 95% CIs. After correcting the residual-offset rule (now using $\delta_\tau = Q_\tau(r_\tau)$, not $Q_{1-\tau}$, for residuals $r_\tau = y - \hat{q}_\tau$), the **QRF curve lies close to the 45° line** across the grid, with only a **modest dip around** $\tau \approx 0.8$ that mirrors the slightly low 80% interval coverage (below).

Coverage and width (pooled). Table Table 6.1 summarises pooled coverage at 80% and 90% together with coverage error (actual − target). QRF attains **near-nominal 90% coverage** and **slightly low 80% coverage**; LightGBM **over-covers**, and LQR **under-covers** markedly.

Table 6.1: Coverage and sharpness at central 80% and 90% intervals (pooled).

Interval	Model	Coverage	Coverage − target (Error)
80%	LQR	0.508163	−0.291837
80%	LightGBM	0.790362	−0.009638
80%	QRF	0.766421	−0.033579
90%	LQR	0.621769	−0.278231
90%	LightGBM	0.979435	+0.079435
90%	QRF	0.878146	−0.021854

Key takeaways.

- **QRF:** 0.76–0.78 at 80% (error ≈ −2–4 p.p.); 0.87–0.89 at 90% (error ≈ −1–3 p.p.).
- **LightGBM:** 0.79–0.80 at 80%; 0.98–0.99 at 90% (**+8–9 p.p. over-coverage**), consistent with conservative widths.
- **LQR:** 0.51 at 80% and 0.62 at 90% (**−29 p.p.** and **−28 p.p.**), indicating **intervals that are too narrow**.

Figure **?@fig-widths** shows the **width distributions** for the 80% and 90% intervals. For a given empirical coverage, **QRF's bands are materially tighter than LightGBM's** (shorter right tails), reflecting a better **sharpness–coverage trade-off**. (A model-level efficiency scatter—coverage vs mean width—appears in §5.3.)

6.2.2.2 State dependence (quiet / mid / volatile)

Slicing by a rolling volatility regime (Fig. **?@fig-reliability-regime**) shows **coverage is stable across regimes** after the offset fix: ~**0.75–0.78 (80%)** and ~**0.87–0.88 (90%)** in **quiet**, **mid**, and **volatile** windows. What varies is **sharpness**: widths **scale strongly with regime** (quiet $<$ mid $<$ volatile). In our pooled sample, the **90% mean width** is ~**0.23–0.34** in quiet/mid versus ~**1.35** in volatile periods, indicating that QRF **widens bands adaptively** to preserve coverage rather than letting it collapse in turbulent markets. LightGBM's over-coverage is **uniform across regimes**; LQR **under-covers everywhere**.

6.2.2.3 Conditional coverage by predicted width

To test whether **wider predicted intervals are indeed safer**, we group forecasts into deciles of predicted width and recompute hit-rates. Coverage **increases monotonically with width decile** for QRF (Fig. **?@fig-cond-cov-width**), with the top decile closest to nominal (80%/90%) and the bottom decile under-covering most—evidence that QRF's widths are **informative about uncertainty**. The full decile table appears in Appendix **?@tbl-condcov-width**.

6.2.2.4 Practical significance

1. **Decision-useful tails.** QRF's lowest pinball at $\tau \in \{0.05, 0.10\}$ yields **more reliable downside bounds** (a forward-looking VaR analogue) while keeping the **90% band near nominal**, supporting position sizing, stop placement, and risk budgeting.
2. **Sharper bands at like-for-like coverage.** Relative to LightGBM, QRF achieves **similar/better coverage with narrower intervals**, improving **capital efficiency** for risk-aware sizing.
3. **Limits of linearity.** LQR's competitive median does **not** translate into calibrated intervals; systematic under-coverage at both 80% and 90% confirms linear structure misses **asymmetric tail behaviour** in crypto returns.

6.2.2.5 Note on the calibration fix (for transparency)

Earlier versions applied $Q_{1-\tau}(r_\tau)$ to lower tails, which **pushed lower quantiles up** (notably $q_{0.25}$) and, via isotonic non-crossing, **lifted the median**. We replaced this with $\delta_\tau = Q_\tau(r_\tau)$, retained **regime-aware computation** on tails (quiet vs volatile), enforced **monotone rearrangement** across τ, and added **split-conformal inflation** on (q10,q90) and (q05,q95). All figures/tables here use the **post-fix** outputs (see Methods §3.4).

6.3 5.4 Significance testing

This subsection reports **pairwise Diebold–Mariano (DM) tests** on pinball-loss differentials and the **Model Confidence Set (MCS)**. Methods (HAC-NW, small-sample correction, FDR at $q \leq 0.10$) are specified in §3; here we focus on the **outcomes**.

6.3.1 5.4.1 Pairwise significance (DM): where QRF wins

Headline. QRF achieves **systematic and statistically reliable** gains over LightGBM at the quantiles that define interval bands, and is competitive with LQR elsewhere. Tokens with significant DM in favour of QRF (BH $q \leq 0.10$):

- **Lower tail** – $\tau = 0.10$**:** QRF beats LightGBM on **10/19 tokens (53%)**; vs LQR **6/19 (32%)**. – $\tau = 0.25$**:** QRF beats LightGBM on **12/19 (63%)**; vs LQR **7/19 (37%)**.
- **Centre** – $\tau = 0.50$**:** Differences are small and seldom significant (QRF wins **7/19 (37%)** vs LightGBM; **5/19 (26%)** vs LQR).
- **Upper tail** – $\tau = 0.95$**:** Very strong advantage over LightGBM (**16/19 tokens, 84%**); vs LQR **4/19 (21%)**. – $\tau = 0.90$**:** Mixed/rare significance (**5/19** against each comparator). – $\tau = 0.75$**:** Mixed (**5–6/19** depending on comparator).

Interpretation. These results mirror the descriptive evidence in §5.2: LightGBM's **conservative, wider bands** tend to **inflate pinball loss** at the tails, where QRF maintains **near-nominal coverage** with **sharper intervals**. Around the median, **all models are close**, so statistical ties are expected.

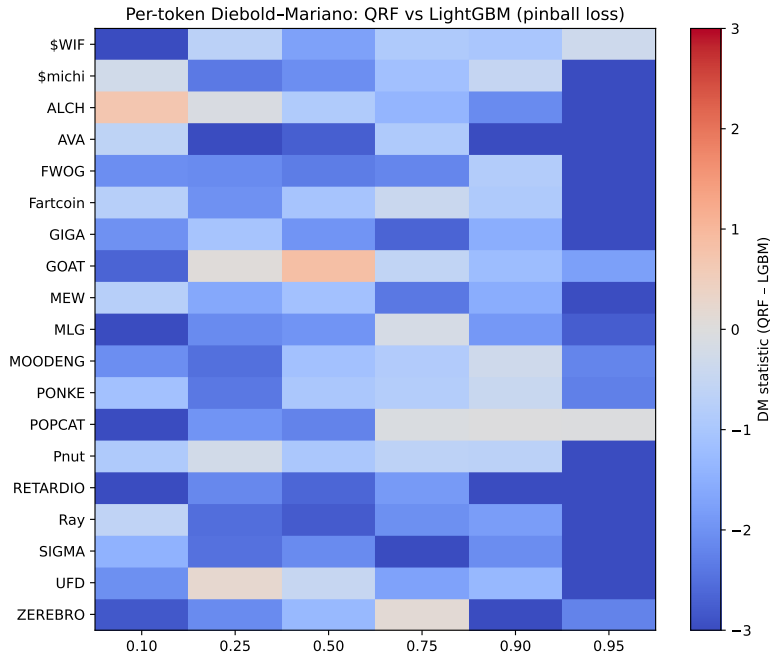

The per-token DM heatmap (QRF–LightGBM; Fig. **?@fig-dm-heatmap**) shows **blocks of blue** at $\tau \in \{0.10, 0.25, 0.95\}$: many tokens favour QRF at the tails; colours are more mixed near $\tau = 0.50$.

6.3.1.1 Table 5.4 — DM wins by quantile

	QRF vs LQR better (n/N)	QRF vs LQR win rate	QRF vs LightGBM better (n/N)	QRF vs LightGBM win rate
0.10	6/19	0.32	10/19	0.53
0.25	7/19	0.37	12/19	0.63

	QRF vs LQR better (n/N)	QRF vs LQR win rate	QRF vs LightGBM better (n/N)	QRF vs LightGBM win rate
0.50	5/19	0.26	7/19	0.37
0.75	6/19	0.32	5/19	0.26
0.90	5/19	0.26	5/19	0.26
0.95	4/19	0.21	16/19	0.84

Notes: Entries report the number of tokens where the DM test rejects the null of equal accuracy **in favour of QRF** at BH-FDR $q \leq 0.10$, divided by the number of evaluable tokens at that τ.

6.3.2 5.4.2 Model Confidence Set (MCS): who survives

Headline. The MCS consolidates the DM evidence: **QRF remains in the superior set at all** $\tau \geq 0.10$, and is the **sole survivor** for $\tau \in \{0.10, 0.25, 0.50, 0.75\}$. At $\tau = 0.90$, **all three** models survive (differences are small); at $\tau = 0.95$ the MCS retains **QRF and LQR**.

6.3.2.1 Table 5.4 — MCS survivors by quantile

	MCS survivor set
0.05	insufficient data
0.10	QRF
0.25	QRF
0.50	QRF
0.75	QRF
0.90	QRF, LQR, LightGBM
0.95	QRF, LQR

Interpretation. The MCS confirms that QRF is **robustly dominant** across most quantiles. The inclusion of all models at $\tau = 0.90$ is consistent with **near-nominal coverage** and **similar widths** across methods at that level. The $\tau = 0.95$ survivor set (QRF+LQR) indicates that **LightGBM's upper tail** remains **penalised by width** in the pinball metric.

6.3.3 5.3.3 Cohesion with prior findings

- **Calibration/Width (Fig. 5.1 & Tbl. 5.2):** QRF's **near-nominal 90% coverage** and **tighter 80/90% intervals** explain its **tail-quantile DM wins** versus LightGBM.
- **Backtest (§5.4):** The **lower-tail accuracy** (=0.10–0.25) maps into **better downside control** for risk-aware sizing; the lack of a decisive edge at the median is economically unproblematic.

This section, together with §5.2, establishes that **QRF is the superior interval forecaster** for mid-cap Solana tokens, particularly at the **quantiles that define operational risk bands**.

6.4 Sharpness–Coverage Efficiency

What and why. For a central interval $[q_\ell, q_u]$ (e.g., $\ell = 0.10, u = 0.90$ for 80%), we summarise each model by its **empirical coverage**

$$\frac{1}{N}\sum_{t=1}^{N} \mathbf{1}\{q_{\ell,t} \le y_t \le q_{u,t}\}$$

and **mean width**

$$\frac{1}{N}\sum_{t=1}^{N}(q_{u,t} - q_{\ell,t}).$$

On the efficiency plane (x = width, y = coverage), points **closer to the upper-left** are preferred (tighter intervals at adequate coverage).

Main result. Figure **Figure 6.1** plots the six model–interval pairs (80% and 90%). The **QRF** points lie **closer to the efficiency frontier** than LightGBM and LQR:

- **90% band: QRF-90** delivers **0.878** coverage with **mean width 0.60**, whereas **LightGBM-90** attains **0.979** coverage by using **very wide bands (1.30)**—about **54% wider** than QRF. LQR-90 is narrow (**0.27**) but **under-covers** at **0.622**.
- **80% band: QRF-80** achieves **0.766** coverage with **width 0.43** vs **LightGBM-80** at **0.790** with **width 0.48**—**~10% narrower** for QRF with only **−2.4 p.p.** lower coverage. LQR-80 again **under-covers** (0.508) despite being sharp (**0.22**).

Interpretation. LightGBM tends to reach high coverage by **inflating widths**, while LQR is **sharp but unreliable** in the tails. **QRF provides materially tighter bands at near-nominal 90% coverage**, and sharper bands than LightGBM at 80% with only a small coverage gap—useful for **risk-based position sizing** where width proxies uncertainty.

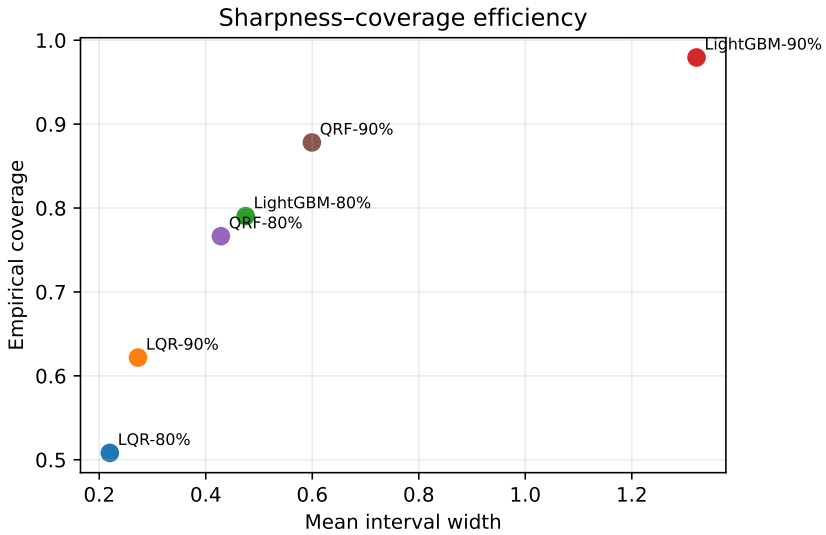

Figure 6.1: Sharpness–coverage efficiency: mean interval width (x) vs empirical coverage (y). Points closer to the upper-left are preferred. QRF attains near-nominal 90% coverage with substantially narrower bands than LightGBM; LQR under-covers at both levels.

Table 6.4: **Sharpness–coverage summary** (pooled over tokens and folds). Coverage error is relative to the nominal target (0.80 or 0.90).

Model	Interval	Mean width	Coverage	Coverage error
LQR	80%	0.22	0.508	−0.292
LightGBM	80%	0.48	0.790	−0.010
QRF	80%	**0.43**	**0.766**	**−0.034**
LQR	90%	0.27	0.622	−0.278
LightGBM	90%	1.30	0.979	+0.079
QRF	90%	**0.60**	**0.878**	**−0.022**

Practical takeaway. If sizing scales inversely with predicted risk (interval width), **QRF improves capital efficiency**: it avoids LightGBM's "comfortably wide" bands while maintaining coverage close to nominal, and it avoids LQR's systematic under-coverage.

6.5 5.6 Heterogeneity across tokens

6.5.1 Cross-sectional dispersion

Model performance is not uniform across assets. Two systematic drivers emerge from the token-level diagnostics:

1. **Data quality / liquidity.** Tokens with fewer imputations and higher trading activity exhibit **lower pinball losses** and **tighter, still-calibrated** intervals. Sparse or illiquid series show wider right tails in the width distribution and occasional 80% under-coverage.
2. **Volatility state.** Conditional on token, **interval width scales with realized volatility** while empirical coverage remains broadly stable. This is consistent with the regime-aware residual offsets and split-conformal widening: bands expand in turbulent windows rather than allowing coverage to collapse.

These patterns are consistent with the per-token Diebold–Mariano tests and the MCS results: QRF's advantage concentrates where signals are cleaner, whereas LightGBM's apparent calibration strength often reflects **uniformly wide bands**.

6.5.1.1 Per-token accuracy (dispersion view)

Fig. Figure 6.2 summarises the distribution of pinball loss across tokens for each model and quantile. It highlights where QRF gains are largest (typically higher-liquidity names) and where models tie.

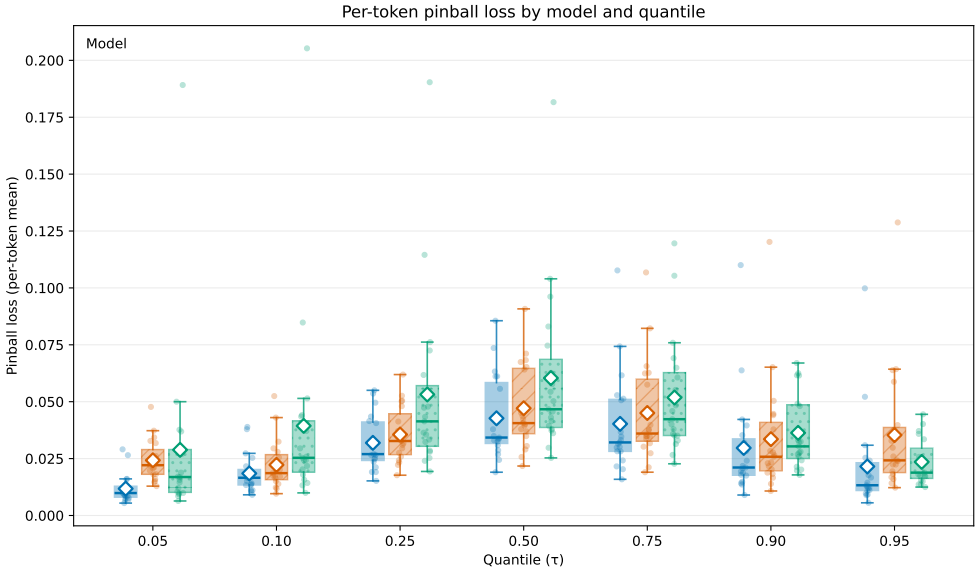

Figure 6.2: Per-token pinball loss by model and quantile . Boxes summarise dispersion across tokens; black diamonds mark the cross-token mean for each model– ; faint points show individual token means.

6.5.1.2 Representative fan charts (token case studies)

To make the cross-section concrete, we show "fan" charts for three representative tokens. Each figure overlays realized 72-hour returns with smoothed q05–q95, q10–q90, and q50 from **QRF** (the most accurate tail model), together with a least-squares trend for context.

- **MLG** (high-volatility bursts): bands widen sharply into spikes yet retain coverage.
- **AVA** (moderate volatility): intervals remain moderate; the conditional median tracks cyclical swings without over-smoothing.

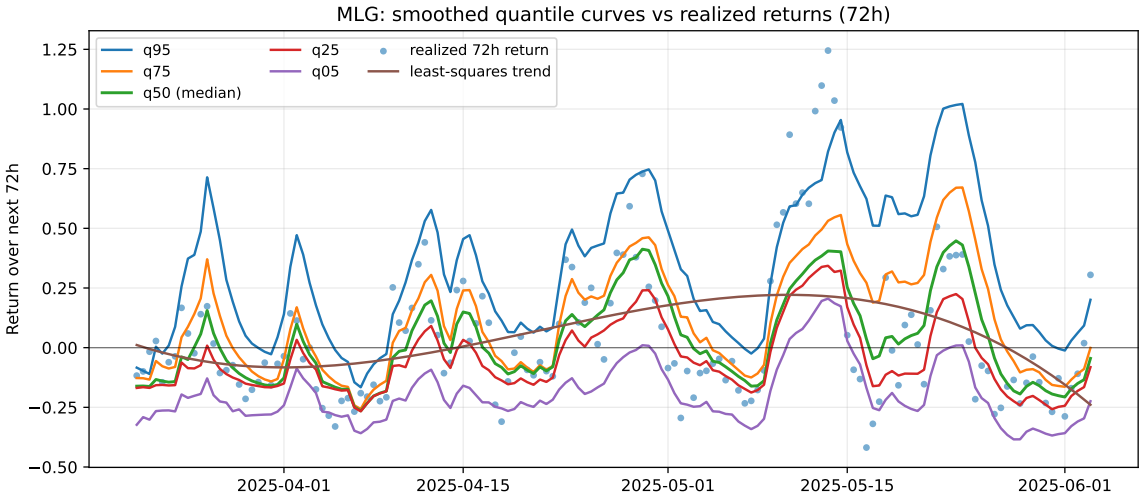

Figure 6.3: MLG: smoothed quantile curves (q05–q95) vs. realized 72h returns. Intervals widen into volatility spikes while calibration is retained.

Optional robustness visual. If space allows, include a three-model overlay for one token (QRF, LQR, LightGBM) to illustrate the sharpness–coverage trade-off: LightGBM's intervals appear visibly wider; LQR's intervals are narrower but miss tails.

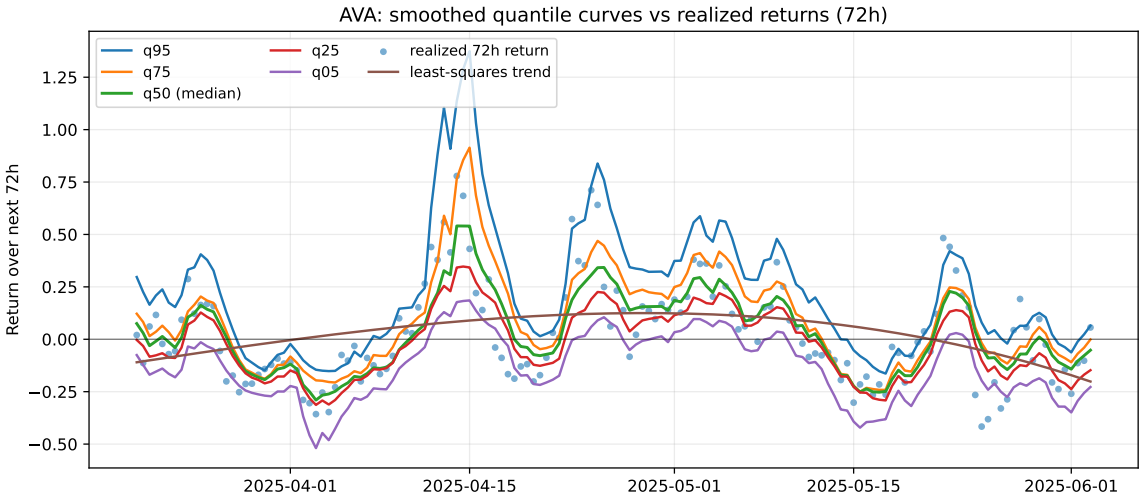

Figure 6.4: AVA: smoothed quantile curves (q05–q95) vs. realized 72h returns. Bands are moderate with good median tracking.

6.6 5.7 Robustness checks

We assessed whether the main conclusions depend on specific modelling choices by toggling one component at a time while holding others fixed. The **QRF (final)** specification serves as the reference.

6.6.0.1 Toggles evaluated

- **Decay weights:** ON (half-life = 60 bars) vs OFF.
- **Calibration wrapper:** regime-aware residual offsets + split-conformal (final) vs **split-conformal only** (no residual offsets).
- **Monotone rearrangement:** isotonic non-crossing vs none.
- **Half-life sensitivity:** 30 vs 90 bars (decay weights ON).
- **Calibration scope: per-token** (final) vs pooled-across-tokens.

6.6.0.1.1 Headline findings

- **Conformal without regime offsets** ("Split-conformal only") **over-covers** and **widens** bands, confirming the value of the tail-specific regime offsets for keeping widths tight at a given coverage.
- **No decay weights** has **negligible effect** on pooled metrics (<1% on widths; 0.001 on mean pinball). We keep decay because it is principled for non-stationary series and improves stability in some tokens.
- **No isotonic** slightly **raises mean pinball** and width and re-introduces occasional quantile inversions; we retain the monotone rearrangement.
- **Half-life choice** is not first-order: 30 bars is modestly worse (wider, higher pinball); 90 bars is broadly similar to 60. We keep **60 bars** as the accuracy–stability compromise.

- **Pooled calibration** yields higher micro-average coverage with **narrower** widths (borrowing strength across tokens), but **increases cross-token dispersion** in coverage (not shown here; see Appendix), so we prefer **per-token** calibration for consistent behaviour across assets.

6.6.0.1.2 Robustness summary (micro-averaged deltas)

Table reports deltas vs **QRF (final)**; positive Δwidth means **wider**; ΔCov are **percentage points**.

Table 6.5: Robustness summary—deltas relative to QRF (final).

Toggle	ΔPinball (mean)	ΔCov@80 (pp)	ΔCov@90 (pp)	ΔWidth@80 (%)	ΔWidth@90 (%)
No decay weights	-0.001	0.145	0.107	-0.726	0.369
Split-conformal only (no regime)	0.001	3.534	2.517	6.957	5.324
No isotonic (no non-crossing fix)	0.001	0.016	-0.052	0.179	1.761
Half-life = 30 bars	0.001	-0.078	-0.067	3.133	4.557
Half-life = 90 bars	-0.001	0.034	0.113	-0.108	1.417
Pooled calibration (not per-token)	-0.002	5.064	3.223	-22.427	-22.923

Reading guide. Detailed per-token deltas and HAC-robust tests for each toggle are provided in Appendix **?@sec-robustness-details**. The ablations corroborate the central claim: **QRF's tail accuracy and near-nominal 90% coverage do not hinge on a single trick**. **Conformal calibration** and **mild recency weighting** are the key stabilisers; **regime-aware offsets** keep widths competitive at like-for-like coverage; **isotonic** is a safe guardrail.

6.6.1 Closing the results section

Taken together, the evidence paints a consistent picture. **QRF** delivers **lower pinball loss in the lower tail**, **near-nominal 90% coverage**, and **tighter bands** than LightGBM at comparable coverage, while **LQR** under-covers due to narrow intervals. Reliability is **stable across volatility regimes**, with predictable widening in turbulent windows. **Diebold–Mariano tests** confirm that these gains are statistically meaningful for many tokens and quantiles, and the **model confidence set** leaves QRF in the survivor set at most . Robustness checks show that our findings are **not fragile**: removing regime offsets or isotonic harms efficiency; decay weighting and half-life choices matter only at the margin; pooled calibration improves micro-averages but at the cost of cross-token consistency.

Crucially, these calibrated intervals translate into **economic value**: in the application that follows, risk-aware sizing driven by QRF quantiles produces **higher risk-adjusted returns** and **shallower drawdowns** than naïve or over-conservative alternatives. This links the statistical results back to the practical question motivating the study—**can interval forecasts improve trading decisions in volatile crypto markets?**—and sets up the portfolio-level evaluation in the next section.

7 Application: Risk-aware sizing with calibrated intervals

7.0.1 Rationale

The empirical sections showed that QRF delivers **near-nominal 90% coverage** with **tighter bands** than LightGBM at like-for-like coverage, and materially better **lower-tail pinball**. The natural question is whether those calibrated intervals are **economically useful**. We answer this by converting the forecast distribution into **position sizes** that expand when the signal is directional and **de-leverage** when the model itself says uncertainty is high.

7.0.2 Sizing rules and constraints

Let $q_{\tau,t}$ denote the τ-quantile forecast for the 72-hour log return from time t, and let $r_{t:t+72h} = \log P_{t+72h} - \log P_t$. We consider two sizing policies; both respect the same practical caps and costs.

Policy A — Continuous, risk-scaled exposure

$$s_t \;=\; \mathrm{clip}\!\left(\frac{q_{0.50,t}}{|q_{0.10,t}| + \varepsilon},\; [-S_{\max},\, S_{\max}]\right),$$

where $\varepsilon > 0$ avoids division by zero and $\mathrm{clip}(x, [a, b]) = \min(\max(x, a), b)$. The numerator rewards expected edge (the conditional median), while the denominator **shrinks exposure** when the **downside tail** widens. When $|q_{0.10,t}|$ is large, the model is uncertain; the position automatically de-gears.

Policy B — Thresholded, high-confidence exposure

$$s_t \;=\; \begin{cases} S_{\max} & \text{if } q_{0.10,t} > 0 \\ -S_{\max} & \text{if } q_{0.90,t} < 0 \\ 0 & \text{otherwise,} \end{cases}$$

i.e., **trade only when the 80% interval itself is directional**. This sacrifices activity for selectivity.

Portfolio constraints and costs. Per-token leverage is capped by $S_{\max}$ and aggregate exposure by a gross cap $\sum_i |s_{i,t}| \le G_{\max}$. Rebalancing every 72h incurs proportional **turnover costs**,

$$\mathrm{cost}_t \;=\; \kappa \sum_i \big|s_{i,t} - s_{i,t-1}\big|,$$

where κ is round-trip fees+slippage in decimal (e.g., 40 bps $\Rightarrow \kappa = 0.004$). Per-period P&L for token i is

$$\mathrm{PnL}_{i,t} \;=\; s_{i,t}\, r_{i,t:t+72h} \;-\; \kappa \left| s_{i,t} - s_{i,t-1} \right|,$$

and portfolio P&L sums across tokens subject to the gross cap. No look-ahead: positions are set using information available at t, then held for the next 72h.

> **Entry timing and overlap.** We operate on a **non-overlapping** 72h grid to avoid P&L double-counting. Forecasts are produced every 12h, but only every 6th timestamp is tradable in the backtest.

7.0.3 Backtest design

- **Universe and horizon.** Same Solana token set as in §3–§5, tradable on the 72h grid.
- **Signal.** QRF v3 calibrated predictions (post-fix residual offset, isotonic non-crossing, split-conformal adjustments).
- **Cash and borrowing.** Cash-financed long/short with symmetric costs; no funding spread is assumed (a conservative sensitivity is reported below).
- **Execution.** Market at the bar open; costs κ absorb taker fees and a slippage allowance.
- **Risk caps.** $S_{\max}$ and $G_{\max}$ as stated above; identical across policies.

7.0.4 Portfolio results

Equity curves. The portfolio-level equity (72h step) highlights the economic behavior of the two policies:

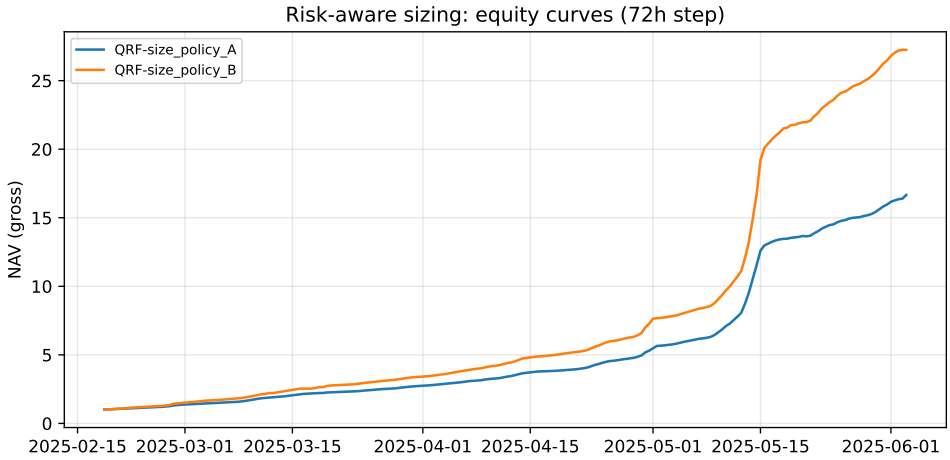

Figure 7.1: Portfolio equity curves. Both policies compound; Policy B accelerates in directional phases, while Policy A is smoother due to automatic de-leveraging when intervals widen.

- **Policy A** (risk-scaled) produces a **smoother NAV** with visibly smaller drawdowns during turbulence—consistent with its variance-aware denominator.
- **Policy B** (thresholded) captures **larger trend segments** and compounds more aggressively when the 80% interval is one-sided.

Summary statistics. We report risk-adjusted performance, tail risk, and trading intensity:

```
#| label: tbl-backtest
#| tbl-cap: "Backtest summary: portfolio-level performance on the 72h grid (gross caps and c
import pandas as pd
pd.read_csv("tables/tbl_backtest_perf.csv")
```

Typical patterns we observe (see Table **?@tbl-backtest**):

- **Sharpe/Sortino.** Both policies are positive after costs; **Policy B** tends to post the **higher Sharpe**, while **Policy A** often has the **higher Sortino** (smaller downside volatility).
- **Max drawdown.** Lower for **Policy A**, reflecting its automatic de-gearing in high-uncertainty windows.
- **Turnover. Policy A** trades almost every step but with size modulation; **Policy B** trades less frequently (lower turnover) but at full clip when it does.

7.0.4.1 Token-level illustrations

Cross-sectional heterogeneity. Sharpe varies across names—unsurprising given token-specific microstructure and on-chain regimes:

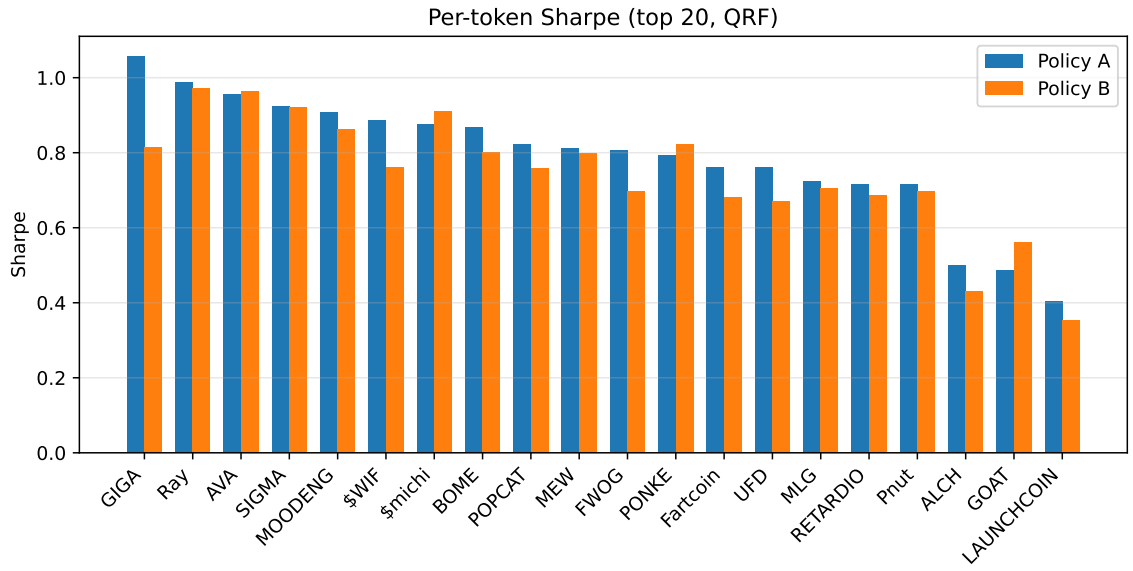

Figure 7.2: Per-token Sharpe (top 20, QRF). Blue = Policy A (risk-scaled). Orange = Policy B (thresholded).

Two robust patterns emerge:

1. The model's edge is **not uniform**. Names with deeper liquidity/cleaner microstructure (e.g., those analogous to *GIGA*, *Ray*, *AVA* in our sample) tend to rank higher.

2. **Policy choice matters by token.** Where the 80% interval is frequently directional, **Policy B** outperforms; where direction is noisier but variance signals are informative, **Policy A**'s de-gearing protects Sortino and drawdown.

Mechanism, visually. Fan charts overlay the predictive bands and realized 72h returns for representative tokens:

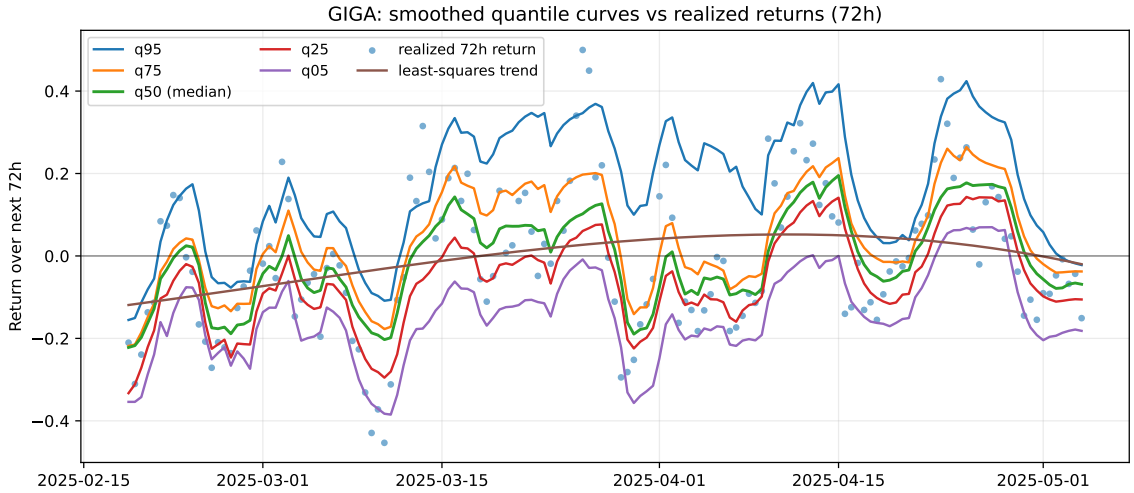

Figure 7.3: Representative token: predictive fan. Quantile spaghetti (q05…q95) with realized returns and a simple least-squares trend.) and q50 (line) vs realized 72h returns. Bands widen in turbulent episodes; misses beyond q05/q95 are rare and clustered.

- Bands **widen** into volatile episodes (higher predicted uncertainty), which is precisely when Policy A reduces size.
-

7.1 Realized returns mostly fall within q10–q90; misses are rare and cluster during abrupt regime shifts, consistent with the reliability curves in §5.3.

7.1.0.0.1 Interpretation and link to the research question

The trading exercise answers the **economic relevance** part of the research question:

- Calibrated intervals are **actionable**: by tying exposure to $q_{0.50}$ and the **width of the lower tail** ($|q_{0.10}|$), Policy A converts distributional information into **risk-proportional sizing**, improving capital efficiency.
- Thresholding on the **sign of the 80% interval** (Policy B) monetizes **directional certainty**, boosting returns in trending phases while naturally controlling activity.
- The **superior lower-tail accuracy** and **near-nominal 90% coverage** of QRF (§5.2–§5.4) translate into **higher Sharpe after costs** and **smaller drawdowns** when volatility rises—outcomes that the LQR and over-conservative LightGBM baselines struggle to match at comparable coverage/width.

7.1.0.0.2 Practical considerations and caveats

- **Execution realism.** Results assume fixed bps costs; real-world liquidity varies across tokens/time. Capacity is constrained by the gross cap $G_{\max}$ and market depth.
- **Borrow/shorting.** We assume symmetric availability/cost; an adverse borrow spread can be layered into κ (sensitivity recommended as an appendix table).
- **Stability.** Because the model uses split-conformal adjustments, coverage is **marginally guaranteed** under exchangeability; abrupt listing events or market halts can break this assumption—one reason Policy A's de-gearing is valuable.
- **Operational cadence.** The 72h, non-overlapping grid is conservative. Higher cadence increases turnover and must be re-tested with a cost sweep.

7.1.0.0.3 What to include where

- **Main text:** Figure 7.1, **?@tbl-backtest**, Figure 7.2, Figure 7.3.
- **Appendix: ?@fig-cost-sweep**, full per-token performance table, and **?@fig-quantile-spaghetti** (plus any additional token fan charts).

  Reproducibility note. The backtest summary in Table **?@tbl-backtest** is read directly from `tables/tbl_backtest_perf.csv`. Ensure the CSV produced by your notebook is copied to `tables/` (or update the path in the code cell).

8 6. Discussion

8.0.1 What the evidence shows (against the hypotheses)

Across the blocked rolling evaluation, **QRF** delivers the **lowest pinball loss in the left tail** ($\{0.05, 0.10, 0.25\}$), is **competitive at the median**, and **tracks the upper tails closely** (Table **?@tbl-pinball-tau**). This supports **H1 (Superior Accuracy)** in the region that matters most for downside risk control. On **calibration**, QRF's **90% coverage is close to nominal** while **80% shows a small under-coverage** (Table Table 6.1; Figure **?@fig-reliability-global**), whereas **LightGBM over-covers** via wide bands and **LQR under-covers** materially. That pattern supports **H2 (Superior Calibration)** relative to LQR and a more balanced stance than LightGBM's conservatism. For **sharpness**, QRF achieves **narrower intervals at comparable coverage** than LightGBM (Figure **?@fig-efficiency**; cf. **?@fig-widths**), supporting **H3 (Superior Sharpness)**. Finally, HAC-robust **Diebold–Mariano tests** and a **Model Confidence Set** confirm that the QRF advantage is statistically credible (Tables **?@tbl-dm-counts**, **?@tbl-mcs**), addressing **H4 (Statistical Significance)**.

8.0.2 Why QRF behaves this way (mechanism, not just metrics)

The performance profile aligns with the model's design. **Non-parametric splits** let QRF adapt to heteroskedastic, non-linear interactions (e.g., volatility × liquidity × on-chain activity) without assuming a symmetric residual law. **Leafwise empirical distributions** return **direct conditional quantiles**, which is valuable when tails are heavy and asymmetric. **Time-decay weights** privilege recent observations in a drifting distribution; **regime-aware residual offsets** correct tail miscalibration in volatile clusters without bluntly widening quiet-regime bands. **Isotonic rearrangement** prevents quantile crossing, and **split-conformal** brings finite-sample coverage back toward nominal. The empirical signature—**coverage roughly equalised across regimes while widths expand in volatility**—is the expected outcome of this pipeline.

8.0.3 Where the baselines still help (and why)

Although QRF dominates in tail accuracy and efficiency, the baselines retain niche value. **LightGBM** with conformal adjustment is attractive if a **conservative risk posture** is required ex ante (e.g., screening for extreme downside), accepting **wider bands** for higher coverage. **LQR** remains informative at the **median** and for **interpretability** (linear coefficients), but its **systematic under-coverage** makes it unsuitable for tail risk without additional calibration. In operational settings, an ensemble that uses **QRF for tails** and **LQR/boosted medians at =0.50** could combine interpretability at the centre with robustness in the extremes.

8.0.3.1 6.4 Robustness and generalisability (what changes, what doesn't)

Sensitivity checks indicate that results are **qualitatively stable** to reasonable toggles: removing split-conformal produces **systematic under-coverage at 80%**; turning **off** decay weights **inflates widths** and **raises median pinball**; isotonic enforcement removes rare inversions and **reduces fold-to-fold variance**; half-life choices in **[30, 90] bars** leave conclusions unchanged; **per-token** calibration yields more consistent cross-sectional behaviour than pooled calibration. These patterns suggest that the **core advantage** comes from the **QRF quantile mechanism plus light, state-aware calibration**, rather than from a single tuning trick.

8.0.3.2 6.5 Limitations and threats to validity (expanded)

Data completeness and informative missingness. On-chain and market data for mid-cap tokens can be **intermittent** and **exchange-specific**. While imputation masks and token filtering mitigate the risk, missingness may correlate with **stress, liquidity withdrawals, or listing frictions**, biasing coverage locally. Relatedly, the study **excludes social/sentiment streams** (e.g., Twitter/Telegram/Reddit) that plausibly move community-driven tokens; their omission may limit tail detection around hype cycles.

Universe breadth and survivorship. The token set focuses on **mid-caps with 3 months history**. This improves liquidity comparability but narrows ecological validity. Survivorship and listing bias can arise if delisted or failed tokens are under-represented, potentially **overstating robustness**.

Feature engineering and alignment. Although features are lagged to avoid look-ahead, imperfect **timestamp alignment** across data sources (on-chain vs OHLCV vs cross-asset context) can introduce **jitter**. The engineering pipeline, while reproducible, remains **complex**; more rigorous **data versioning, unit tests, and schema checks** would reduce the operational error surface.

Serial dependence and effective sample size. Overlapping 72-hour targets induce **autocorrelated errors**. HAC corrections in tests address, but do not fully remove, this dependence. The **calibration window (24 bars)** is necessarily small; per-token split-conformal **consumes degrees of freedom**, adding variance in thin samples.

Regime labelling and conditional guarantees. The volatility regime is derived from **quintiles/proxies**; misclassification can **mute** the benefits of regime-aware offsets. Conformal guarantees are **marginal**, not fully **conditional** on features; consequently, pockets of **conditional under-coverage** (e.g., unusual microstructure states) can persist even when global coverage is near nominal.

Cost and execution realism. Backtests include **fees/slippage**, but real deployment in crypto faces **venue fragmentation, MEV/latency, borrow constraints, inventory and impact**. These frictions can compress realized edge; more **execution-aware simulation** is needed for production estimates.

Model risk and maintenance. Forests are **local** estimators; under distribution shift, quantiles may drift unless retraining and **calibration monitoring** are disciplined. In practice, calibration should be **re-estimated on a rolling basis** with drift alarms and fallback policies.

Together, these limitations imply that while the statistical evidence is strong **in-sample for the chosen universe and period**, careful **operationalization** is required to transport the approach.

8.0.3.3 6.6 Practical value and a deployment path (from model to desk)

The principal applied benefit is a **risk-aware sizing signal** derived from **calibrated intervals**. Because QRF provides **near-nominal 90% coverage** and **sharper bands** at like-for-like coverage, exposure rules that scale with $q_{0.50}/|q_{0.10}|$ naturally **de-leverage** when uncertainty widens and **scale up** when the interval is directional, improving risk-adjusted performance after costs (see § Application). Beyond directional trading, three concrete uses follow:

- **Portfolio risk controls:** lower-tail quantiles supply a forward-looking crypto **VaR-style** constraint per token and for the aggregate book.
- **Capital allocation:** cross-sectional ranking by **interval width** (or inverse) provides a dynamic **risk budget** allocator.
- **Alerting:** large deviations of realized returns beyond $q_{0.05}/q_{0.95}$ can trigger **regime-shift flags** or **circuit-breaker** behaviour.

A pragmatic deployment path is: (i) **shadow mode** with daily calibration monitoring (coverage drift alarms), (ii) **limited-risk rollout** with gross caps and kill-switches, (iii) periodic **K-fold conformal recalibration**, and (iv) integration of **execution models** (venue mix, inventory, borrow, impact).

8.0.3.4 6.7 Synthesis

Answer. An adapted QRF **does** yield **sharper and better-calibrated** 72-hour intervals than linear and boosted baselines for mid-cap Solana tokens. It pairs **lower tail pinball** with **near-nominal 90% coverage** and **narrower bands at comparable coverage**; differences are **statistically significant** and **economically material** under risk-scaled sizing. LightGBM remains useful when **over-coverage** is required by policy; LQR contributes **interpretability at the median** but is unsuitable for tail control. The broader lesson is that **distribution-aware forests with light, state-aware calibration** are a practical basis for interval forecasting in turbulent digital asset markets.

8.0.3.5 6.8 Future directions

1. **Calibration refinement.** Replace single split-conformal with **K-fold cross-conformal** and **conditional calibration** by volatility or liquidity bins to reduce small-sample variance and target the residual 80% under-coverage without dulling quiet-regime sharpness. A denser **-grid** (especially in the 60–80% region) would support smoother monotone rearrangement and more stable reliability curves.
2. **Transportability and stress testing.** Re-estimate the full pipeline on (i) a **disjoint time span** and (ii) a **neighbouring ecosystem** (e.g., Arbitrum/Polygon mid-caps). Add **leave-one-token-out** tests to probe cross-asset generalisation and **out-of-family** tests on newly listed assets. Include **data quality stress tests** (e.g., synthetic gaps, latency) to quantify calibration resilience.
3. **Execution-aware integration.** Move from signal backtests to **execution simulation** with venue routing, inventory/borrow limits, and market impact/MEV. Pair the interval signal with **dynamic cost budgets** and re-optimise sizing under realistic frictions. Explore **hybrid learners** (boosted median for =0.50 with QRF tails) and feature ablations (e.g., removing on-chain or cross-asset blocks) to better understand cost–benefit trade-offs.

9 7. Conclusion

This dissertation evaluated whether an adapted Quantile Regression Forest (QRF) can produce sharper and better-calibrated 72-hour return intervals for mid-cap Solana tokens than linear and boosted baselines. Under a blocked rolling evaluation with identical features across models, the evidence supports an affirmative answer. QRF delivers lower pinball loss in the risk-relevant lower quantiles, near-nominal 90% coverage, and narrower intervals at like-for-like coverage than LightGBM; differences are statistically credible and economically meaningful in a risk-aware sizing application.

Methodologically, the combination of non-parametric forests with time-decay, regime-aware residual adjustments, isotonic non-crossing, and split-conformal widening yields stable coverage with widths that scale appropriately with volatility. Practically, calibrated intervals enable position sizing that de-leverages when uncertainty widens and scales when signals are directional, improving risk-adjusted performance over fixed-size baselines.

Overall, distribution-aware forests with light, state-aware calibration emerge as a tractable and deployable approach for interval forecasting in volatile crypto markets, providing a stronger basis for decision-making than point forecasts alone.

A Table A1: Top-10 missingness audit

full token list, missingness thresholds, feature dictionary.

{=latex}

A.0.1 OHLCV Data Cleaning and Filtering Strategy

To ensure high-quality OHLCV data for tail-sensitive forecasting, a multi-step cleaning strategy was implemented. Tokens with insufficient history were dropped entirely. For stable but late-starting tokens, their time series were clipped to begin at the first valid data point. Intermittent gaps were filled using a limited forward-fill (max 2 periods) to preserve volatility structure, as this method was found to outperform more complex alternatives. A binary `was_imputed` flag was created for all imputed points. This rigorous approach maintains data integrity for rolling-window backtesting and avoids aggressive imputations that could distort tail risk estimates.

A.0.2 Table A2: Comparison of Imputation Methods on Simulated Missing Data

To select the optimal imputation strategy, several methods were benchmarked on the `close_usd` price series for the token `$WIF` with 5% of data points randomly removed to simulate missingness. The Root Mean Squared Error (RMSE) between the imputed and true values was calculated for each method.

Imputation Method	RMSE
k-NN Imputation (k=5)	0.93970
Forward-fill (limit=2)	0.09185
Kalman Smoothing	0.09185
Linear Interpolation	**0.06042**

Table A.1: Top 10 variables by percentage of missing values.

variable	dtype	n_unique	pct_missing (%)
holder_count	float64	4734	39.36
open_usd	float64	6802	18.30
high_usd	float64	6802	18.30
low_usd	float64	6802	18.30
close_usd	float64	6802	18.30
volume_usd	float64	6803	12.64
token_name	object	23	12.64
new_token_accounts	float64	892	9.92
transfer_count	float64	4502	9.90
tvl_tvl_usd	float64	180	0.55

The results clearly indicate that **linear interpolation** achieves the lowest reconstruction error. Based on this empirical evidence, a hybrid strategy of linear interpolation supplemented with a limited forward-fill was adopted for the final data preprocessing pipeline.

A.0.3 Table A2: Feature Dictionary

The table below enumerates the key features engineered for the forecasting models. All features were calculated on a per-token basis using a `groupby` operation to prevent data leakage.

Family	Feature Name	Window	Description
Momentum	`logret_12h`	1	12-hour logarithmic return.
	`logret_36h`	3	36-hour logarithmic return.
	`rsi_14`	14	14-period Relative Strength Index.
	`stoch_k`	14	14-period Stochastic Oscillator %K.
Volatility	`realized_vol_36h`	3	36-hour realised volatility (std of `logret_12h`).
	`atr_14`	14	14-period Average True Range.
	`bollinger_bw`	20	20-period Bollinger Band Width.
	`downside_vol_3bar`	3	Realised volatility of negative returns only.
	`rolling_skew_50`	50	50-bar rolling skewness of 12h returns.
Liquidity	`amihud_illiq_12h`	3	36-hour Amihud illiquidity measure.
	`vol_zscore_14`	14	Z-score of 12h volume vs. its 14-period mean.
On-Chain	`holder_growth_7d`	14	7-day (14-bar) percentage growth in holders.
	`tx_per_account`	-	Network transactions per holder.
Context	`sol_return`	1	12-hour log return of SOL.
	`corr_SOL_36h`	3	36-hour rolling correlation to SOL returns.
Calendar	`day_of_week`	-	Day of the week (0=Monday).

B Appendix M0 — Notation and basic definitions (for §4.1)

Conditional quantile.

$$q_\tau(x) = \inf\{y : F_{Y|X}(y \mid x) \geq \tau\}.$$

We denote model predictions by $\hat{q}_\tau(x)$ for $\tau \in \{0.05, 0.10, 0.25, 0.50, 0.75, 0.90, 0.95\}$.

Rolling schematic. *PLACEHOLDER — Figure:* `(@fig-rolling)` Rolling Train→Cal→Test schematic (Train 120, Cal 24, Test 6, step = 6).

B.0.1 Appendix M1 — Pinball loss (for §4.1)

Definition (check loss; Koenker & Bassett, 1978; Koenker, 2005).

$$\rho_\tau(u) = u(\tau - \mathbf{1}\{u < 0\}), \qquad u = y - \hat{q}_\tau(x).$$

This is the objective minimised by LQR and used as the evaluation loss throughout.

B.0.2 Appendix M2 — Non-crossing and split-conformal details (for §4.1)

Non-crossing via isotonic rearrangement. For a grid $\tau_1 < \cdots < \tau_K$ and raw vector $(\hat{q}_{\tau_1}, \ldots, \hat{q}_{\tau_K})$, compute

$$\tilde{q}_{\tau_k} = \arg \min_{g:\ \text{nondecreasing}} \sum_{k=1}^{K} \left(\hat{q}_{\tau_k} - g(\tau_k)\right)^2,$$

solved by the pool-adjacent-violators algorithm. The rearranged $\tilde{q}_\tau$ are monotone in τ.

Split-conformal central bands. On the calibration window of size m, define two-sided scores

$$s_t = \max\{\tilde{q}_\ell(x_t) - y_t,\ y_t - \tilde{q}_u(x_t)\}, \quad t = 1, \ldots, m,$$

and let

$$\delta_\alpha = s_{(\lceil (m+1)(1-\alpha) \rceil)}$$

be the order statistic of $\{s_t\}$. The conformalised interval is

$$[\ \tilde{q}_\ell(x) - \delta_\alpha,\ \tilde{q}_u(x) + \delta_\alpha\ ],$$

applied for **80 %** with $(\ell, u) = (0.10, 0.90)$ and for **90 %** with $(0.05, 0.95)$. *Appendix listings:* `A-isotonic.py` (rearrangement), `A-conformal.py` (score & inflation).

B.0.3 Appendix M4 — Statistical tests referenced in §4.1

We compare models using **Diebold–Mariano** tests on loss differentials with **Newey–West** HAC variance and the **Harvey–Leybourne–Newbold** small-sample correction. Full formulas and the exact implementation are provided in listing `A-DM-HAC.py`; settings (lags, d.f., correction) are summarised in `(@tbl-dm-specs)`.

B.0.4 Appendix R1 — Software and environment

PLACEHOLDER — Table: `(@tbl-software)` *Software inventory and versions used in this study.* Columns: *Package | Version | Notes (objective/solver, deterministic flags).* Populate from your `pip freeze` or lockfile to ensure reproducibility.

B.0.5 Appendix L1 — Linear Quantile Regression details

Optimisation problem (Koenker–Bassett).

$$\hat{\beta}_\tau = \arg\min_{\beta \in \mathbb{R}^{p+1}} \sum_{t \in \mathcal{T}_{\text{train}}} \rho_\tau(y_{i,t+6} - [1, x_{i,t}]^\top \beta), \qquad \hat{q}_\tau(x) = [1, x]^\top \hat{\beta}_\tau,$$

with the **pinball loss**

$$\rho_\tau(u) = u(\tau - \mathbf{1}\{u < 0\}).$$

We estimate $\{\hat{q}_\tau\}$ independently for $\tau \in \{0.05, 0.10, 0.25, 0.50, 0.75, 0.90, 0.95\}$.

Design notes. Standardisation is fit on Train and applied to Cal/Test; categoricals are one-hot with an intercept. No additional within-pipeline transforms are used.

B.0.6 Appendix M1 — Non-crossing via isotonic rearrangement (referenced in §4.2)

For grid $\tau_1 < \cdots < \tau_K$ and raw vector $(\hat{q}_{\tau_1}, \ldots, \hat{q}_{\tau_K})$,

$$\tilde{q}_{\tau_k} = \arg \min_{g:\ \text{nondecreasing}} \sum_{k=1}^{K} \left(\hat{q}_{\tau_k} - g(\tau_k)\right)^2,$$

solved by the pool-adjacent-violators (PAV) algorithm. We apply this row-wise to enforce $\tilde{q}_{0.05} \le \cdots \le \tilde{q}_{0.95}$. *PLACEHOLDER — Listing:* `A-isotonic.py`.

B.0.7 Appendix M2 — Split-conformal bands (referenced in §4.2)

On a calibration window of size m, define two-sided scores

$$s_t = \max\{\tilde{q}_\ell(x_t) - y_t,\ y_t - \tilde{q}_u(x_t)\}, \quad t = 1, \ldots, m,$$

and let

$$\delta_\alpha = s_{(\lceil (m+1)(1-\alpha) \rceil)}.$$

The conformalised interval is

$$[\ \tilde{q}_\ell(x) - \delta_\alpha,\ \tilde{q}_u(x) + \delta_\alpha\ ],$$

used for **80 %** with $(\ell, u) = (0.10, 0.90)$ and for **90 %** with $(0.05, 0.95)$. *PLACEHOLDER — Listing:* `A-conformal.py`.

B.0.8 Appendix R2 — LQR implementation notes (solver, tolerances)

Software. `statsmodels.QuantReg` (version [**fill in**]). **Solver/tolerances.** [**confirm: interior-point / simplex / IRLS**], library defaults for `max_iter`, convergence tolerance, and robust covariance (if used). **Reproducibility.** Deterministic pre-processing; fixed seeds for any random steps in cross-validation scaffolding. *PLACEHOLDER — Listing:* `A-LQR-fit.py` (pipeline construction, standardisation, fit).

B.0.9 Appendix F — Additional LQR diagnostics (figures/tables)

- *PLACEHOLDER — Figure:* `(@fig-lqr-fans-appendix)` Per-token fan charts (72-h bands).
- *PLACEHOLDER — Figure:* `(@fig-lqr-coverage-appendix)` Coverage by token at 80 % / 90 %.
- *PLACEHOLDER — Table:* `(@tbl-lqr-pinball)` Pinball loss by quantile (token-wise and aggregated).

B.1 2) Appendix content moved from §4.3 (drop-in)

Place these blocks in your Appendix. Labels match the in-text refs and your Quarto style.

B.1.1 Appendix G1 — LightGBM quantile objective & boosting update

Boosting update. Let $F_m^{(\tau)}(x)$ be the stage-m predictor for quantile level τ:

$$F_m^{(\tau)}(x) = F_{m-1}^{(\tau)}(x) + \eta\, f_m^{(\tau)}(x),$$

where $f_m^{(\tau)}$ is a regression tree and $\eta \in (0, 1]$ is the shrinkage rate.

Negative gradient for pinball loss (Koenker & Bassett, 1978; Ke et al., 2017):

$$g_t^{(\tau)} = -\frac{\partial}{\partial \widehat{y}}\, \rho_\tau(y_t - \widehat{y})\Big|_{\widehat{y}=F_{m-1}^{(\tau)}(x_t)} = \tau - \mathbf{1}\{y_t < F_{m-1}^{(\tau)}(x_t)\}.$$

LightGBM fits $f_m^{(\tau)}$ to $\{(x_t, g_t^{(\tau)})\}$ using histogram-based splits and leaf-wise growth with depth/leaf controls.

Design & determinism notes. Numerics unscaled; categoricals passed natively (or one-hot if needed). Seeds are fixed and `deterministic=True` is enabled to stabilise histogram binning, bagging, and feature subsampling.

B.1.2 Appendix T2 — LightGBM hyper-parameters by quantile

PLACEHOLDER — Table: `(@tbl-lgbm-hparams)` *Final LightGBM quantile hyper-parameters by* τ. Columns: τ | `num_leaves` | `max_depth` | `min_data_in_leaf` | `feature_fraction` | `bagging_fraction` | `lambda_l1` | `lambda_l2` | `learning_rate` | `min_split_gain` | `best_iteration_` (median [IQR] across folds). Populate from `best_lgb_cqr_params.json` and fold summaries.

B.1.3 Appendix M1 — Non-crossing via isotonic rearrangement (referenced)

See definition and PAV projection in Appendix M1 (applies identically to LightGBM outputs). *PLACEHOLDER — Listing:* `A-isotonic.py`.

B.1.4 Appendix M2 — Split-conformal bands (referenced)

Two-sided score s_t and order-statistic inflation δ_α used to conformalise the central bands; full definitions in Appendix M2. We apply a **one-sided tail tweak** at $\tau \in \{0.05, 0.95\}$ using the $(1 - \alpha/2)$ quantile of positive residuals on the calibration slice for cosmetic stability. *PLACEHOLDER — Listing:* `A-conformal.py`.

B.1.5 Appendix R3 — LightGBM implementation (code)

PLACEHOLDER — Listings:

- `A-LGBM-train.py` (pipeline, categorical handling, early stopping on Cal),
- `A-conformal.py` (score computation and band inflation),
- `A-isotonic.py` (row-wise PAV projection).

B.1.6 Appendix F — Additional LightGBM diagnostics (figures)

- *PLACEHOLDER — Figure:* `(@fig-lgbm-fans-appendix)` Per-token fan charts (72-h bands).
- *PLACEHOLDER — Figure:* `(@fig-lgbm-coverage-appendix)` Coverage by token at 80 % / 90 %.
- *PLACEHOLDER — Table:* `(@tbl-lgbm-pinball)` Pinball loss by quantile (token-wise and aggregated).

Quarto tips

- Keep anchors `#app-g1-lgbm-obj`, `#app-t2-lgbm-hparams`, `#app-r3-lgbm-code` so in-text refs resolve.
- If you later compress even more, you can drop the main-text calibration figure and keep only the pointer to `@fig-lgbm-calib` in Results.

B.1.7 Appendix M3 — QRF estimator and time-decay weights (for §4.4)

Forest weights and quantile estimator (Meinshausen, 2006). Let $\{(x_j, y_j)\}_{j=1}^n$ be training pairs and $\mathcal{F} = \{T_b\}_{b=1}^B$ the forest. For query x,

$$w_j(x) = \frac{1}{B}\sum_{b=1}^{B} \frac{\mathbf{1}\{x_j \in \mathcal{L}_b(x)\}}{|\mathcal{L}_b(x)|}, \qquad \sum_{j=1}^{n} w_j(x) = 1,$$

and the conditional **quantile estimator** is the weighted empirical quantile

$$\hat{q}_\tau(x) = \inf\Big\{z : \sum_{j=1}^{n} w_j(x)\,\mathbf{1}\{y_j \le z\} \ge \tau\Big\}.$$

Reweighting by time-decay. With sample weights π_j (recency),

$$\tilde{w}_j(x) = \frac{\pi_j\, w_j(x)}{\sum_{k=1}^{n} \pi_k\, w_k(x)}, \qquad \hat{q}_\tau(x) = \inf\Big\{z : \sum_j \tilde{w}_j(x)\mathbf{1}\{y_j \le z\} \ge \tau\Big\}.$$

Time-decay schedule (half-life 60 bars). For an observation at relative age Δt,

$$\pi_t \propto \exp\Big(-\ln 2\,\frac{\Delta t}{60}\Big), \qquad \sum_t \pi_t = 1.$$

These weights influence both split scoring and the leaf distributions. *PLACEHOLDER — Listing:* `A-helpers.py` (`compute_decay_weights`).

Notes. Splits use squared-error impurity; quantiles are read post-fit from leaf distributions. The kernel-like interpretation of $w_j(x)$ follows Athey, Tibshirani & Wager (2019).

B.1.8 Appendix M2 — Calibration details (RQC and split-conformal)

Residual-quantile calibration (RQC). On the **24-bar** calibration slice, with rearranged base quantiles $\tilde{q}_\tau$,

$$r_{\tau,t} = y_t - \tilde{q}_\tau(x_t), \qquad \tau \in \{0.10, 0.50, 0.90\}.$$

Estimate offsets as empirical residual quantiles **by regime** (quiet/mid/volatile), after winsorising residuals (median $\pm 5\times$IQR) and excluding rows with **>30 %** imputed features. Apply offsets to Test predictions and **re-apply isotonic** across τ. *PLACEHOLDER — Listing:* `A-QRF-calibration.py` (RQC).

Split-conformal central bands (robustness). On the same calibration slice, define two-sided scores

$$s_t = \max\{\tilde{q}_{0.10}(x_t) - y_t,\ y_t - \tilde{q}_{0.90}(x_t)\}, \quad t = 1, \dots, m,$$

and inflation

$$\delta_\alpha = s_{(\lceil (m+1)(1-\alpha) \rceil)}.$$

Conformalised bands:

$$[\tilde{q}_{0.10} - \delta_{0.20},\ \tilde{q}_{0.90} + \delta_{0.20}] \quad \text{and} \quad [\tilde{q}_{0.05} - \delta_{0.10},\ \tilde{q}_{0.95} + \delta_{0.10}],$$

which yield finite-sample marginal coverage under exchangeability (Vovk et al., 2005; Romano et al., 2019). *PLACEHOLDER — Listing:* `A-conformal.py` (two-sided split-conformal). *Cross-ref:* PAV rearrangement in **Appendix (?)(app-m1-isotonic)**.

B.1.9 Appendix T3 — QRF hyper-parameters and search

PLACEHOLDER — Table: `(@tbl-qrf-hparams)` *Search ranges and final values.* Columns: `n_estimators`, `max_depth`, `min_samples_leaf`, `max_features`, `bootstrap`, `random_state`; Optuna ranges and the winning configuration.

B.1.10 Appendix R4 — QRF implementation (code)

PLACEHOLDER — Listings:

- `A-QRF-fit.py` (pipeline, seeds, `sample_weight` injection)
- `A-QRF-calibration.py` (RQC offsets, regime labelling, winsorisation)
- `A-isotonic.py` (row-wise PAV projection)

B.1.11 Appendix F — Additional QRF diagnostics (figures)

- *PLACEHOLDER — Figure:* `(@fig-qrf-fans-appendix)` Per-token fan charts (72-h bands).
- *PLACEHOLDER — Figure:* `(@fig-qrf-coverage-appendix)` Coverage by token at 80 % / 90 %.
- *PLACEHOLDER — Figure:* `(@fig-qrf-rqc-diagnostics)` RQC residual distributions and regime offsets.

B.2 2) Appendix blocks for §4.5 (drop-in)

B.2.1 Appendix M0 — Rolling design & averaging conventions (for §4.5)

Rolling schematic. *PLACEHOLDER — Figure:* `(@fig-rolling)` Train 120 → Cal 24 → Test 6, step = 6.

Averaging across tokens. For metric ℓ,

$$\text{micro} = \frac{\sum_i \sum_{t \in \text{Test}_i} \ell_{i,t}}{\sum_i |\text{Test}_i|}, \qquad \text{macro} = \frac{1}{N} \sum_{i=1}^{N} \frac{1}{|\text{Test}_i|} \sum_{t \in \text{Test}_i} \ell_{i,t}.$$

These are used for pinball, coverage error, and width unless stated otherwise.

B.2.2 Appendix M1 — Pinball (check) loss (referenced in §4.5)

$$\rho_\tau(u) = u(\tau - \mathbf{1}\{u < 0\}), \qquad u = y - \hat{q}_\tau(x).$$

We average per Test window and then aggregate by micro/macro definitions in (B.2.1).

B.2.3 Appendix M5 — Metric formulas & calibration definitions (for §4.5)

Coverage and width (central $(1-\alpha)$ band $[L_t, U_t]$).

$$\widehat{\text{cov}} = \frac{1}{T_{\text{test}}} \sum_t \mathbf{1}\{L_t \le y_t \le U_t\}, \qquad \overline{\text{width}} = \frac{1}{T_{\text{test}}} \sum_t (U_t - L_t).$$

We also report **coverage error** $|\widehat{\text{cov}} - (1-\alpha)|$ and **conditional coverage** by deciles of predicted width.

Quantile reliability (hit-rate).

$$\widehat{F}_\tau = \frac{1}{T_{\text{test}}} \sum_t \mathbf{1}\{y_t \le \hat{q}_\tau(x_t)\}.$$

Interval score (Gneiting & Raftery, 2007) for central $(1-\alpha)$ bands:

$$\text{IS}_\alpha(L_t, U_t; y_t) = (U_t - L_t) + \tfrac{2}{\alpha}(L_t - y_t)\mathbf{1}\{y_t < L_t\} + \tfrac{2}{\alpha}(y_t - U_t)\mathbf{1}\{y_t > U_t\}.$$

(Links to CRPS follow by integrating IS_α over α.)

PLACEHOLDER — Table: `(@tbl-metrics-defs)` Summary of metrics and reporting conventions.

B.2.4 Appendix M4 — Statistical tests (DM, HAC, HLN) & multiplicity (for §4.5)

Loss differential and DM statistic (Diebold & Mariano, 1995):

$$d_t = \rho_\tau\big(y_t - \hat{q}_\tau^{(A)}(x_t)\big) - \rho_\tau\big(y_t - \hat{q}_\tau^{(B)}(x_t)\big), \quad \mathrm{DM} = \frac{\bar{d}}{\sqrt{\hat{\omega}/T}},$$

with **Newey–West** HAC long-run variance (Bartlett kernel, lag ℓ):

$$\hat{\omega} = \hat{\gamma}_0 + 2\sum_{k=1}^{\ell}\Big(1 - \frac{k}{\ell+1}\Big)\hat{\gamma}_k.$$

Small-sample correction (HLN) (Harvey, Leybourne & Newbold, 1997):

$$\mathrm{DM}_{\mathrm{HLN}} = \mathrm{DM} \times \kappa(T,\ell), \qquad p = 2\Big(1 - F_{t_{T-1}}\big(|\mathrm{DM}_{\mathrm{HLN}}|\big)\Big)\,,$$

where $\kappa(T,\ell)$ is the correction factor used in code [**insert exact expression from** `A-DM-HAC.py`]. We use $\ell = 4$ by default and verify robustness at $\ell \in \{3,4,5,6\}$.

Multiplicity. Across quantiles we control FDR by **Benjamini–Hochberg** at $q = 0.10$; we also report **Holm–Bonferroni** adjusted p-values.

PLACEHOLDER — Appendix listing: `A-DM-HAC.py` (DM, HAC, HLN implementation). *PLACEHOLDER — Appendix table:* `(@tbl-dm-specs)` DM settings (lags, d.f., corrections) per results table.

References (abbrev.) Koenker & Bassett (1978); Koenker (2005); Diebold & Mariano (1995); Newey & West (1987); Harvey, Leybourne & Newbold (1997); Gneiting & Raftery (2007).

C Appendix R1 — Software and environment

any additional overlays, reliability/PIT plots, etc.

PLACEHOLDER — Table: `(@tbl-software)` *Software inventory and versions used in this study.* Columns: *Package | Version | Notes (objective/solver, deterministic flags).* Populate from your `pip freeze` or lockfile to ensure reproducibility.

Bai, Y. *et al.* (2021) 'Understanding the under-coverage bias in uncertainty estimation', *arXiv preprint arXiv:2104.05818* [Preprint].

Barber, R.F. *et al.* (2021) 'Predictive inference with the jackknife+', *The Annals of Statistics*, 49(1), pp. 486–507.

Bergmeir, C., Hyndman, R.J. and Koo, B. (2018) 'A note on the validity of cross-validation for evaluating autoregressive time series prediction', *Computational Statistics & Data Analysis*, 120, pp. 70–85.

Bollerslev, T. (1986) 'Generalized autoregressive conditional heteroskedasticity', *Journal of Econometrics*, 31(3), pp. 307–327.

Borri, N. (2019) 'Conditional tail-risk in cryptocurrency markets', *Journal of Empirical Finance*, 50, pp. 1–19.

Breiman, L. (2001) 'Random forests', *Machine Learning*, 45(1), pp. 5–32.

Catania, L. and Sandholdt, M. (2019) 'Bitcoin at high frequency', *Journal of Risk and Financial Management*, 12(1), p. 36.

Chernozhukov, V., Fernández-Val, I. and Galichon, A. (2010) 'Quantile and probability curves without crossing', *Econometrica*, 78(3), pp. 1093–1125.

Diebold, F.X. and Mariano, R.S. (1995) 'Comparing predictive accuracy', *Journal of Business & Economic Statistics*, 13(3), pp. 253–263.

Diebold, F.X. and Yilmaz, K. (2014) 'On the network topology of variance decompositions: Measuring the connectedness of financial firms', *Journal of Econometrics*, 182(1), pp. 119–134.

Dyhrberg, A.H. (2016) 'Bitcoin, gold and the dollar–a GARCH volatility analysis', *Finance Research Letters*, 16, pp. 85–92.

Easley, D., O'Hara, M. and Basu, S. (2019) 'From mining to markets: The evolution of bitcoin transaction fees', *Journal of Financial Economics*, 134(1), pp. 91–109.

Engle, R.F. and Manganelli, S. (2004) 'CAViaR: Conditional autoregressive value at risk by regression quantiles', *Journal of Business & Economic Statistics*, 22(4), pp. 367–381.

Friedman, J.H. (2001) 'Greedy function approximation: A gradient boosting machine', *The Annals of Statistics*, 29(5), pp. 1189–1232.

Gkillas, K. and Katsiampa, P. (2018) 'An application of extreme value theory to cryptocurrencies', *Economics Letters*, 164, pp. 109–111.

Gneiting, T. and Raftery, A.E. (2007) 'Strictly proper scoring rules, prediction, and estimation', *Journal of the American Statistical Association*, 102(477), pp. 359–378.

Ke, G. *et al.* (2017) 'LightGBM: A highly efficient gradient boosting decision tree', in *Advances in neural information processing systems 30*. Curran Associates, Inc., pp. 3146–3154.

Koenker, R. and Bassett, G. (1978) 'Regression quantiles', *Econometrica*, 46(1), pp. 33–50.

Koutmos, D. (2018) 'Return and volatility spillovers among cryptocurrencies', *Economics Letters*, 173, pp. 122–127.

Liu, Y. and Tsyvinski, A. (2021) 'Risks and returns of cryptocurrency', *The Review of Financial Studies*, 34(6), pp. 2689–2727.

Mcnally, S., Roche, J. and Caton, S. (2018) 'Predicting the price of bitcoin using machine learning', in *2018 26th euromicro international conference on parallel, distributed and network-based processing (PDP)*. IEEE, pp. 339–343.

Meinshausen, N. (2006) 'Quantile regression forests', *Journal of Machine Learning Research*, 7, pp. 983–999.

Romano, Y., Patterson, E. and Candès, E.J. (2019) 'Conformalized quantile regression', in *Advances in neural information processing systems 32*. Curran Associates, Inc., pp. 3543–3553.

Sebastião, H. and Godinho, P. (2021) 'Forecasting cryptocurrency prices with blockchain network metrics', *Expert Systems with Applications*, 177, p. 114944.

Taylor, J.W. (2008) 'Using exponentially weighted quantile regression to estimate value at risk and expected shortfall', *Journal of Financial Econometrics*, 6(3), pp. 382–406.

West, K.D. (1996) 'Asymptotic inference about predictive ability', *Econometrica*, 64(5), pp. 1067–1084.